Excitation Transfer in Photosynthetic Systems

Klaus Schulten, Thorsten Ritz, Ana Damjanović, Melih Sener

The content of these lectures is posted on the website
`http://www.ks.uiuc.edu/Research/psu/lecture.html`

December 6, 2000

General Theory

Heuristic Introduction to Excitation Transfer

In the following, we will discuss electronic excitation transfer (ET) according to the following scheme

$$D^* + A \rightarrow D + A^* \; . \tag{1}$$

Here, D and A are assumed to be two spatially seperated molecules. Initially, molecule D is in an excited state ψ_D^* and molecule A in its ground state ψ_A. The Coulomb interaction V_{DA} between these two molecules leads to a reaction where molecule D is deexcited and molecule A is simultaneously excited, thus leading to an excitation transfer from D to A.

It is instructive to investigate the above excitation transfer reaction for a situation in which the relevant molecular system can be modeled as a two-level system. The Hamiltonian of this system is given by

$$H = \begin{pmatrix} E_D & V_{DA} \\ V_{DA} & E_A \end{pmatrix} \; , \tag{2}$$

where E_D, E_A denote the excitation energies of ψ_D^* and ψ_A^*, respectively. Solving the eigenvalue problem for H, one obtains the eigenvectors

$$\Psi_+ = \cos\alpha \; \psi_D^* \psi_A + \sin\alpha \; \psi_D \psi_A^* \tag{3}$$

$$\Psi_- = \sin\alpha \; \psi_D^* \psi_A - \cos\alpha \; \psi_D \psi_A^* \; , \tag{4}$$

with the so-called mixing angle α defined as

$$\alpha = \frac{1}{2} \arctan \left(\frac{2|V_{DA}|}{|\Delta E|} \right) \tag{5}$$

and the corresponding energies

$$E_\pm = \frac{1}{2}(E_D + E_A) \pm \frac{V_{DA}}{\sin 2\alpha} = \frac{1}{2}(E_D + E_A) \pm \frac{|\Delta E|}{\cos 2\alpha} \; , \tag{6}$$

where we defined $\Delta E = E_D - E_A$.

One can verify the above solution to the eigenvalue problem of the two-level quantum system by using the given eigenvectors as ansatz and employing the trigonometic relationship

$$\sin^2 2\alpha = \frac{\tan^2 2\alpha}{1 + \tan^2 2\alpha} \; . \tag{7}$$

For the discussion of excitation transfer, the time dependent Schrödinger equation

$$-\frac{\hbar}{i} \frac{\partial \Phi(\vec{r}, t)}{\partial t} = H \Phi(\vec{r}, t) \tag{8}$$

has to be solved. The time evolution of the eigenstates is given by

$$\Phi_{\pm} = \Psi_{\pm} \exp[-(i/\hbar)E_{\pm}t] \; . \tag{9}$$

A general solution for (8) can be expressed as a linear combination of $\Phi_{\pm}$,

$$\Phi(t) = c_{+}\Phi_{+} \exp[-(i/\hbar)E_{+}t] \; + \; c_{-}\Phi_{-} \exp[-(i/\hbar)E_{-}t] \tag{10}$$

with constant coefficients c_{+}, c_{-} determined by the initial conditions. If we assume that only molecule D is excited at $t = 0$, we have $c_{+} = \cos\alpha$ and $c_{-} = \sin\alpha$, as can be seen from (4). The solution $\Phi(t)$ represents back and forth oscillation of the excitation between the molecules D and A. A straightforward calculation leads to

$$\begin{aligned} \Phi(t) \;\; &= \;\; \exp[-i/\hbar\bar{E}t] \left[\left(\cos\frac{V_{DA}t}{\hbar \sin 2\alpha} - i\cos 2\alpha \cdot \sin\frac{V_{DA}t}{\hbar \sin 2\alpha} \right) |i\rangle \;\; - \right. & (11) \\ &\left. - \; i \sin 2\alpha \cdot \sin\frac{V_{DA}t}{\hbar \sin 2\alpha} |f\rangle \right] \; . & (12) \end{aligned}$$

Here, $\bar{E} = 1/2(E_{+} + E_{-})$ is the average energy of the eigenstates and $|i\rangle, |f\rangle$ denote the initial and final states for excitation transfer, defined as

$$\begin{aligned} |i\rangle \;\; &= \;\; \Psi_{D^*} \, \Psi_A \\ |f\rangle \;\; &= \;\; \Psi_D \, \Psi_{A^*} \; . \end{aligned} \tag{13}$$

From (12), we obtain the expectation value ρ_f of $|f\rangle$,

$$\rho_f(t) = \sin^2 2\alpha \cdot \sin^2 \frac{V_{DA}t}{\hbar \sin 2\alpha} \; . \tag{14}$$

For sufficiently short times, this becomes

$$\rho_f(t) \approx \frac{V_{DA}^2 t^2}{\hbar^2} \; , \tag{15}$$

which is independent of the mixing angle α.

Resonance Case: Delocalized Excitation

The maximum value of $\rho_f(t)$ is

$$\rho_f(t)^{max} = \sin^2 2\alpha = \frac{4V_{DA}^2}{\Delta E^2 + 4V_{DA}^2} \; , \tag{16}$$

which only becomes large for $|V_{DA}| >> |\Delta E|$. This resonance condition corresponds to the value $\alpha = \pi/4$. The first maximum of $\rho_f(t)$ is obtained at the time

$$t^{max} = \frac{h}{4|V_{DA}|} \sin 2\alpha \; . \tag{17}$$

If we define, following Förster, the transfer rate k_{DA} as the maximum expectation value of $\rho_f(t)$ divided by this time, we obtain

$$k_{DA} = \frac{4|V_{DA}|}{h}|\sin 2\alpha| \ . \tag{18}$$

Under resonance conditions $\alpha = \pi/4$, this becomes

$$k_{DA} = \frac{4|V_{DA}|}{h} \ , \tag{19}$$

which is generally regarded as the transfer rate for resonance. The definition of a transfer rate is, however, somewhat problematic in this case. For one, the expectation value $\rho_f(t)$ increases quadratically in time, so that the definition of the transfer rate will change, if a different time constant than the time t^{max} corresponding to the first maximum of $\rho_f(t)$ is chosen. Furthermore, if we evaluate the eigenvectors for the resonance case, we find

$$\Psi_+ = \frac{1}{\sqrt{2}}(\psi_D^*\psi_A + \psi_D\psi_A^*) \tag{20}$$

$$\Psi_- = \frac{1}{\sqrt{2}}(\psi_D^*\psi_A - \psi_D\psi_A^*) \ , \tag{21}$$

with corresponding energy eigenvalues

$$E_\pm = \frac{1}{2}\Delta E \pm V_{DA} \ . \tag{22}$$

The wavefunctions are the symmetric and antisymmetric combinations of the locally excited configurations and the excitation is distributed equally over both molecules. Such a wavefunction which extends over an aggregate (in this case a molecule dimer) is called an *exciton*. The exciton dynamics is coherent and excitation will be transferred back and forth between the molecules, which makes it virtually impossible perform an experiment by which such a transfer rate could be measured. Only when the coherency of the exciton breaks down, due to inter- and intramolecular relaxation, will excitation be localized on one of the molecules and can transfer rates be observed. The resonance transfer rate is an upper limit for the transfer rate between two molecules. We note that the rate is linear in the interaction strength V_{DA} and equal to the splitting between the exciton levels E_+ and E_-, divided by $h/2$.

Non-Resonance Case: Excitation Transfer

In the limiting case that the coupling between the molecules is weak,
$|V_{DA}| << |\Delta E|$, the eigenfunctions of (2) are given by

$$\Psi_+ = \psi_D^*\psi_A \tag{23}$$

$$\Psi_- = \psi_D\psi_A^* \ . \tag{24}$$

This is the nonresonance case, where the excitation is essentially localized either in the one or the other molecule. It is for this weak coupling case, that Förster has derived his theory of excitation transfer. We present here his heuristic introduction of the rate for excitation transfer in the case of very weak couplings.

Let us consider the case that excited molecule D occupies the vibrational level v and unexcited molecule A occupies the vibrational level w. (For an energy level structure which includes vibrational levels, cf. Fig. 1 and the following section). We will now consider that collisional processes between the molecule and its environment occur. Such processes are responsible for the fast establishment of equilibrium between the vibrational degrees of freedom of an excited molecule and its protein surroundings. If the coupling is so weak that the transfer has not been accomplished during the collisional lifetime of such a vibronic level, the transfer will necessarily be affected by such collisions. Under these conditions, transfer between the vibrational levels of two molecules can solely occur with the exchange of the vibrational quanta v and w between both molecules. The increasing expectation value for the final state of the system, which may be designated here as ρ_{Dv,A^*w}, can be calculated from (15) if we replace there the electronic interaction energy V_{DA} by the vibronic interaction energy $V_{Dw,Av}$. Thus, we get

$$\rho_{Dv,A^*w} \approx \frac{V_{Dv,Aw}^2 t^2}{\hbar^2} \tag{25}$$

as long as no collision occurs. If the first collision occurs at $t = \tau$, then ρ_{Dv,A^*w} will have increased by the amount of

$$\Delta\rho_{Dv,A^*w} \approx \frac{V_{Dv,Aw}^2 \tau^2}{\hbar^2} \ . \tag{26}$$

Since such a collision destroys all phase relations between the wavefunctions, the increase during further collision time periods will be the same, so that we get

$$\rho_{Dv,A^*w}(t) \approx \frac{t}{\tau}\Delta\rho_{Dv,A^*w} \approx \frac{V_{Dv,Aw}^2 \tau}{\hbar^2} t \ . \tag{27}$$

The transfer rate is now linear in time and can be unambiguously calculated as

$$k_{DA}^{vw} \approx \frac{\rho_{Dv,A^*w}(t)}{t} = \frac{V_{Dv,Aw}^2 \tau}{\hbar^2} \ . \tag{28}$$

The characteristic feature of this very weak coupling case is the quadratic dependence of the transfer rate on the interaction energy, as opposed to the linear dependence for the resonant or strong coupling case.

Förster Theory

Thermal fluctuations and protein movements give rise to intramolecular vibrations of the donr and acceptor molecules. An energy level scheme that takes these vibrational states into account

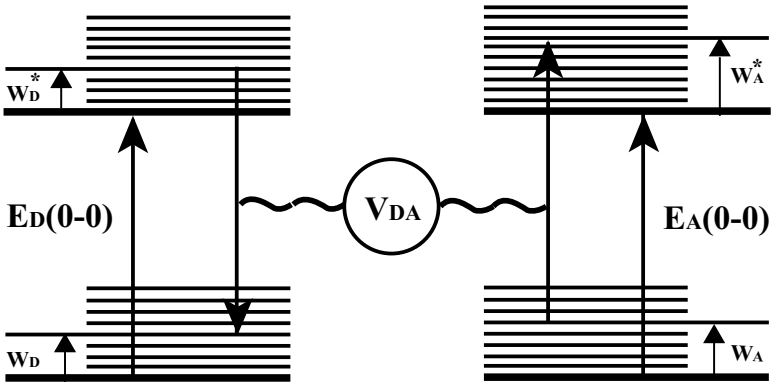

Figure 1: Energy level scheme of a donor and of an acceptor molecule. The energies w_D, w_D^* w_A and w_A^* describe the continuum vibrational and bath states associated with the ground and the excited states of donor and acceptor, respectively. The energy that is transferred between the donor and the acceptor is denoted by E, while $E_D(0-0)$ and $E_A(0-0)$ label the zero-zero transition energies of donor and of acceptor respectively.

is displayed in Figure 1. For each electronic transition (D, D^*, A, A^*), there exists a continuous spectrum of vibrational states. The energy difference of each vibrational state to the respective electronic state is denoted by $\omega_D, \omega_D^*, \omega_A, \omega_A^*$.

In this scheme, excitation transfer is described as occuring from a manifold of vibrational and bath states, associated with the excited electronic state of the donor, into a manifold of vibrational and bath states associated with the electronic ground state of the acceptor. The wavefunctions of the initial and the final states can be expressed, in the Born-Oppenheimer approximation, as a product of the electronic wavefuncion ψ and of the vibrational wavefunction χ,

$$\Psi_{D^*}\,\Psi_A \;=\; \psi_{D^*}\,\psi_A\,\chi(w_D^*)\,\chi(w_A) \tag{29}$$

$$\Psi_D\,\Psi_{A^*} \;=\; \psi_D\,\psi_{A^*}\,\chi(w_D)\,\chi(w_A^*)\;. \tag{30}$$

We assume now that the electronic coupling V_{DA} is so weak that inter- and intramolecular relaxation processes occur on a timescale faster than excitation transfer. This assumption justifies the use of first-order time dependent perturbation theory to derive the excitation transfer rate, leading to a Golden Rule rate expression for excitation transfer.

Fermi's Golden Rule is derived in the attached lecture notes, which are also posted on the website http://www.ks.uiuc.edu/research/psu/lecture.html. It states that the rate of transfer of electronic excitation from donor D to acceptor A can be evaluated as

$$k_{DA} \;=\; \frac{2\,\pi}{\hbar}\,|U_{DA}|^2\,\rho_{DA}\;. \tag{31}$$

Here U_{DA} describes the electronic coupling between donor and acceptor; ρ_{DA} represents the density of states available for the transition with dimension 1/energy. This density is related to the electronic transitions involved in the energy transfer, *i.e.*, the deexcitation of the donor from an electronically excited state S_n to its ground state S_0 and the excitation of the acceptor from its ground state S_0 to its excitted state S_m. The density arises from vibrational motion coupled to the two transitions, *i.e.*, calculation of ρ_{DA} requires an account of the participation of vibration in the respective electronic transitions.

We consider first a single electronic transition, say $S_0 \rightarrow S_1$ of the acceptor. We will assume here and throughout the lecture that donor and acceptor vibrations at the moment of the transitions are in thermal equilibrium. For this case, we know that the vibrational state densities are populated according to the Boltzmann distribution and we can write ρ_{DA} excplicitely

$$\begin{aligned} k_{DA} &= \frac{2\,\pi}{\hbar} \int_{E=0}^{\infty} dE \int_{w_A=0}^{\infty} dw_A \int_{w_D^*=0}^{\infty} dw_D^* \\ &\times \left[\frac{g_D^*(w_D^*)\, exp(-w_D^*/k_BT)}{Z_D^*}\right] \left[\frac{g_A(w_A)\, exp(-w_A/k_BT)}{Z_A}\right] |\tilde{U}_{DA}|^2 \,. \end{aligned} \tag{32}$$

Here, $g_D^*(w_D^*)$ and $g_A(w_A)$ denote the multiplicity of the vibrational levels and Z_D^*, Z_A are the partition functions defined as

$$\begin{aligned} Z_D^* &= \int_{w_D^*=0}^{\infty} dw_D^*\, g_D^*(w_D^*)\, exp(-w_D^*/k_BT) \,, \\ Z_A &= \int_{w_A=0}^{\infty} dw_A\, g_A^*(w_A)\, exp(-w_A/k_BT) \end{aligned} \tag{33}$$

The interaction matrix $\tilde{U}_{DA}$ in (33) can be expressed as

$$\tilde{U}_{DA} = \langle \Psi_{D^*} \Psi_A \,|V_{DA}|\Psi_D\, \Psi_{A^*}\rangle \,. \tag{34}$$

Here, as above, V_{DA} represents the Coulomb interaction that causes the transition. The wavefunctions of the initial and the final states can be expressed, in the Born-Oppenheimer approximation, as a product of the electronic wavefuncion ψ and of the vibrational wavefunction χ,

$$\Psi_{D^*}\, \Psi_A = \psi_{D^*}\, \psi_A\, \chi(w_D^*)\, \chi(w_A) \tag{35}$$

$$\Psi_D\, \Psi_{A^*} = \psi_D\, \psi_{A^*}\, \chi(w_D)\, \chi(w_A^*) \,. \tag{36}$$

The interaction matrix $\tilde{U}_{DA}$ can in turn be expressed as a product of the purely electronic part, and two vibrational overlap terms (Franck-Condon factors)

$$\tilde{U}_{DA} = \langle \psi_{D^*}\psi_A \,|V_{DA}|\psi_D\, \psi_{A^*}\rangle\, \langle \chi(w_D^*)|\chi(w_D)\rangle\, \langle \chi(w_A)|\chi(w_A^*)\rangle \,. \tag{37}$$

The rate for excitation transfer k_{DA} can now be rewritten as

$$k_{DA} \;=\; \frac{2\,\pi}{\hbar}\,|U_{DA}|^2 \int\limits_{E=0}^{\infty} dE\,G_D(E)\,G_A(E)\;, \tag{38}$$

where $U_{DA} = \langle \psi_{D^*}\psi_A\,|V_{DA}|\psi_D\,\psi_{A^*}\rangle$ is the purely electronic part of the coupling which does not depend on any of the integration parameters. $G_D(E)$ and $G_A(E)$ are defined as

$$\begin{aligned} G_D(E) \;&=\; \int\limits_{w_D^*=0}^{\infty} dw_D^* \left[\frac{g_D^*(w_D^*)\,exp(-w_D^*/k_BT)\,|\langle\chi(w_D^*)|\chi(w_D)\rangle|^2}{Z_D^*}\right] \\ G_A(E) \;&=\; \int\limits_{w_A=0}^{\infty} dw_A \left[\frac{g_A(w_A)\,exp(-w_A/k_BT)|\langle\chi(w_A)|\chi(w_A^*)\rangle|^2}{Z_A}\right]\;, \end{aligned} \tag{39}$$

where

$$\begin{aligned} w_D \;&=\; E_D(0-0) + w_D^* - E \\ w_A^* \;&=\; -E_A(0-0) + w_A + E\;. \end{aligned} \tag{40}$$

By virtue of definition, $G_D(E)$ and $G_A(E)$ are normalized to unity on an energy scale.

$G_D(E)$ and $G_A(E)$ are closely related to the spectroscopic transition probabilities between ground and excited states within molecules D and A. Following Förster, we start from the definition of Einstein's coefficients for emission

$$A_D(E) \;=\; \frac{4\,n}{3\,\hbar^4 c^3}\,E^3 \int\limits_{w_D^*=0}^{\infty} dw_D^* \frac{g_D^*(w_D^*)\,exp(-w_D^*/k_BT)}{Z_D^*}\,|\vec{D}(E_D(0-0)-E+w_D^*, w_D^*)|^2\;, \tag{41}$$

and for absorption

$$B_A(E) \;=\; \frac{2\,\pi}{3\,n^2\hbar^2} \int\limits_{w_A=0}^{\infty} dw_A \frac{g_A(w_A)\,exp(-w_A/k_BT)}{Z_A}\,|\vec{D}(w_A, E-E_A(0-0)+w_A)|^2\;. \tag{42}$$

Here, c denotes the speed of light, n denotes the refractive index and $\vec{D}(E_D(0-0)-E+w_D^*, w_D^*)$, $\vec{D}(w_A, E-E_A(0-0)+w_A)$ are the transition dipole moments for the donor's emission and acceptor's absorption, respectively. These transition dipole moments can, analogous to the couplings, be expressed as a product of a purely electronic term and a vibrational term,

$$\begin{aligned} \vec{D}(E_D(0-0)-E+w_D^*, w_D^*) \;&=\; \vec{D}_D\,\langle\chi(w_D^*+E_D(0-0)-E)|\chi(w_D^*)\rangle \\ \vec{D}(w_A, E-E_A(0-0)+w_A) \;&=\; \vec{D}_A\,\langle\chi(w_A)|\chi(w_A-E_A(0-0)+E)\rangle\;. \end{aligned} \tag{43}$$

Einstein's coefficients are related to experimentally measurable quantities through well-known expressions. For emission,

$$A_D(E) \;=\; \frac{1}{\tau_0}\,f_D(E)\;, \tag{44}$$

where τ_0 is the radiative lifetime of the donor excited state and $f_D(E)$ is the emission spectrum normalized to unity on an energy scale. For absorption,

$$B_A(E) \;=\; \frac{c\ln 10}{n\,N}\;\frac{1}{E}\;\varepsilon_A(E)\;, \tag{45}$$

where $N = 6.022{\cdot}10^{20}$ is the number of molecules per millimol and $\varepsilon_A(E)$ is the molar extinction coefficient of the acceptor's absorption.

Inserting (43-45) into (41),(42) and comparing with the definition of $G_D(E)$ and $G_A(E)$ in (39), one arrives at the relations

$$\begin{aligned} G_D(E) &= N_D\;\frac{f_D(E)}{E^3} \\ G_A(E) &= N_A\;\frac{\varepsilon_A(E)}{E}\;. \end{aligned} \tag{46}$$

The normalization constants N_D, N_A are defined as

$$\begin{aligned} N_D &= \frac{4\,n\,\tau_0}{3\,\hbar^4 c^3}\;|\vec{D}_D|^2 \\ N_A &= \frac{2\pi\,N}{3\ln 10\,\hbar^2\,n\,c}\;|\vec{D}_A|^2\;. \end{aligned} \tag{47}$$

Due to above mentioned normalization of the spectral densities $G_D(E)$ and $G_A(E)$ to unity, the normalization constants N_D, N_A can be evaluated by integrating over the respective spectral functions,

$$\begin{aligned} N_D &= \left(\int_{E=0}^{\infty} dE\;\frac{f_D(E)}{E^3}\right)^{-1} \\ N_A &= \left(\int_{E=0}^{\infty} de\;\frac{\varepsilon_A(E)}{E}\right)^{-1} \end{aligned} \tag{48}$$

Thus, the functions $G_D(E)$ and $G_A(E)$ can be determined entirely from the data available through spectroscopic measurements. In order to determine the rate of excitation transfer according to (38), one is left with evaluating the electronic interaction matrix U_{DA}. Before we turn to evaluating U_{DA}, we will revisit the derivation of the rate expression from Fermi's Golden Rule to elucidate the physics of excitation transfer better.

An Alternative Look at Fermi's Golden Rule

We start, as above, from Fermi's Golden Rule

$$k_{DA} \;=\; \frac{2\,\pi}{\hbar}\;|U_{DA}|^2\;\rho_{DA}\;. \tag{49}$$

For the sake of simplicity we now assume that the vibrations can be described classically and that a single vibrational mode participates; the latter assumption an be readily generalized. In order to make an analytical description possible we assume that the vibration is governed in the electronic ground state by the harmonic potential

$$V_{A,0}(q) \;=\; \frac{1}{2} f_A q^2 \tag{50}$$

and in the excited state by

$$V_{A,1}(q) \;=\; \frac{1}{2} f_A (q \;-\; q_A)^2 \;+\; \epsilon_A \tag{51}$$

In order to induce a spectral transition at position q one needs to impart an energy E

$$E \;=\; V_{A,1}(q) \;-\; V_{A,0}(q) \;=\; \frac{1}{2} f_A q_A^2 \;-\; f_A q_A q \;+\; \epsilon \tag{52}$$

One can conclude that if one imparts an energy E, the ytransition takes place at position $q(E)$ given by

$$q(E) \;=\; \frac{\frac{1}{2} f_A q_A^2 \;-\; E \;+\; \epsilon}{f_A q_A} \; . \tag{53}$$

The probability that the acceptor is found at coordinate q is given by the Boltzmann distribution

$$p(q) \;=\; \sqrt{f_a / 4\pi k_B T} \, \exp[-f_A q^2 / 2 k_B T] \; . \tag{54}$$

where the prefactor is chosen to normalize the distribution, i.e., to enforce

$$\int_{-\infty}^{+\infty} dq \; p(q) \;=\; 1 \; . \tag{55}$$

Accordingly, the probability that the system absorbs energy E is given by

$$S_A(E) \;=\; p[q(E)] |dq/dE| \; , \tag{56}$$

where the Jacobian factor $|dq/dE|$ enforces the normalization

$$\int_{-\infty}^{+\infty} dE \; S_A(E) \;=\; 1 \; . \tag{57}$$

Combining Eqs. (53, 54, 57) results in

$$S_A(E) \;=\; \sqrt{1/2\pi\sigma_A} \, \exp[-(\frac{1}{2} f_A q_A^2 \;-\; E \;+\; \epsilon)^2 / \sigma^2] \tag{58}$$

where

$$\sigma \;=\; q_A \sqrt{f_A k_B T} \; . \tag{59}$$

We note that $S_A(E)$ can be interpreted as the absorption spectrum of the acceptor; according to the condition (57) it has the dimension $1/E$, i.e., that of an energy density $\rho(E)$.

One can similarly establish the emission spectrum for the donor. In fact, one can apply the expression (58) above, replacing $E \rightarrow -E$ and $\epsilon \rightarrow -\epsilon$, i.e.,

$$S_D(E) \;=\; \sqrt{1/2\pi\sigma_D}\,\exp[-(\frac{1}{2}f_D q_D^2 \;+\; E \;-\; \epsilon)^2/\sigma^2] \tag{60}$$

where

$$\sigma \;=\; q_D\,\sqrt{f_D k_B T}\;. \tag{61}$$

Now the probability that the acceptor absorbs energy E_A and the donor emits energy E_D is the product $S_A(E_A)\,S_D(E_D)$; such process requires energy $E \;=\; E_A - E_D$. There are many ways to achive this energy balance, e.g., namely for $E \;=\; (E_A + \epsilon(-(E_D + \epsilon)$. Accounting for all these possibilities requires adding all probabilities, i.e., the total probability that energy E is used in an acceptor absorption / donor emission process is

$$S_{AD}(E) \;=\; \int_{-\infty}^{+\infty} dE_1\,S_A(E_1)\,S_D(E_1 \;-\; E)\;. \tag{62}$$

In case of a thermal transition, i.e., without a thermal energy source, the probability for an acceptor / donor transition is

$$S_{AD}(0) \;=\; \int_{-\infty}^{+\infty} dE\,S_A(E)\,S_D(E)\;. \tag{63}$$

We can therefore state that the rate for an energy transfer process in which acceptor A gets electronically excited and donor D gets electronically deexcited is

$$k_{DA} \;=\; \frac{2\,\pi}{\hbar}\;|U_{DA}|^2\;\int_{-\infty}^{+\infty} dE\,S_A(E)\,S_D(E)\;, \tag{64}$$

where $S_D(E)$ and $S_A(E)$ define the normalized donor emission and acceptor absorption spectra, respectively.

In case that the shape of the spectra are not known, one can approximate, rather crudely, $S_D(E)$ and $S_A(E)$ in (64) by Gaussians

$$\begin{aligned} S_{D(A)}(E) \quad &=\quad (2\,\pi\,\sigma_{D(A)}^2)^{-1/2} \\ &\times\quad \exp\,[-\,(E \;-\; E_{D(A)})^2/2\,\sigma_{D(A)}^2] \end{aligned} \tag{65}$$

where $\sigma_{D(A)} \;=\; (\Gamma_{D(A)}/2)\;(2\,\ln 2)^{-1/2}$. $E_{D(A)}$ is the energy of the emission or absorption maximum and $\Gamma_{D(A)}$ is the full width at half-maximum. The values of $E_{D(A)}$ and $\Gamma_{D(A)}$ are estimated from the observed emission and absorption spectra.

Electronic Coupling for Excitation Transfer

The electronic coupling U_{DA} in (64, 38) arises from the Coulomb interaction in the donor-acceptor pair. This interaction can be expressed

$$\frac{1}{2} \sum_{\substack{m,n,p,q \\ \in I_D \cup I_A}} \sum_{\sigma,\sigma'} \; (\phi_m \phi_n | \phi_p \phi_q) \; c^\dagger_{m\sigma} \, c^\dagger_{p\sigma'} \, c_{q\sigma'} \, c_{n\sigma} \tag{66}$$

where $c^\dagger_{m\sigma}$, $c_{n\sigma'}$ denote the fermion creation and annihilation operators which create and annihilate, respectively, electrons with spins σ and σ' in the mutually orthogonal atomic orbitals ϕ_m and ϕ_n. I_D, I_A denote the set of atomic orbital indices of the donor and acceptor molecules, and we defined

$$(\phi_m \phi_p | \phi_n \phi_q) = \iint d\vec{r}_1 \, d\vec{r}_2 \; \phi^*_m(\vec{r}_1) \, \phi_p(\vec{r}_1) \; \frac{e^2}{|\vec{r}_1 - \vec{r}_2|} \; \phi^*_n(\vec{r}_2) \, \phi_q(\vec{r}_2) \; . \tag{67}$$

The intramolecular contributions to (66), arising from the sums $\sum_{m,n,p,q \in I_D}$ and $\sum_{m,n,p,q \in I_A}$, are accounted for in determining the intramolecular (donor, acceptor) electronic excitations; the intermolecular contributions, e.g., $\sum_{m,p \in I_D, n,q \in I_A}$ and $\sum_{m,q \in I_D, n,p \in I_A}$, are the perturbations which induce the electronic excitation transfer as described by (38). These contributions can be written, exploiting the anticommutation properties of fermion operators,

$$\begin{aligned} \hat{V} \;\; = \;\; & \sum_{\substack{i,j, \in I_D \\ \sigma}} \sum_{\substack{R,S, \in I_A \\ \sigma'}} \Big[(\phi_i \phi_j | \phi_R \phi_S) \; c^\dagger_{i\sigma} c_{j\sigma} \; c^\dagger_{R\sigma'} c_{S\sigma'} \\ & \qquad - (\phi_i \phi_S | \phi_R \phi_j) \; c^\dagger_{i\sigma} c_{j\sigma'} \; c^\dagger_{R\sigma'} c_{S\sigma} \Big] \; . \end{aligned} \tag{68}$$

The initial and final electronic states involved in the excitation transfer are assumed to be products of intramolecular donor and acceptor ground and excited states $|\Psi_D\rangle$, $|\Psi^*_D\rangle$, $|\Psi_A\rangle$, $|\Psi^*_A\rangle$, namely, $|\text{init}\rangle = |\Psi^*_D\rangle \otimes |\Psi_A\rangle$ and $|\text{fin}\rangle = |\Psi_D\rangle \otimes |\Psi^*_A\rangle$. The electronic coupling U_{DA} in (38) can then be expressed by the matrix element

$$U_{DA} \;=\; \langle \text{init} | \hat{V} | \text{fin} \rangle \tag{69}$$

which can be evaluated using (68). The result can be split into two contributions

$$U_{DA} \;=\; U^c_{DA} \;+\; U^{ex}_{DA} \tag{70}$$

where

$$\begin{aligned} U^c_{DA} \;\; = \;\; & \sum_{\substack{i,j \\ \in I_D}} \sum_{\substack{R,S \\ \in I_A}} (\phi_i \phi_j | \phi_R \phi_S) \\ \times \;\; & \langle \Psi^*_D | \sum_\sigma \, c^\dagger_{i\sigma} \, c_{j\sigma} | \Psi_D \rangle \; \langle \Psi_A | \sum_{\sigma'} \, c^\dagger_{R\sigma'} \, c_{S\sigma'} | \Psi^*_A \rangle \end{aligned} \tag{71}$$

describes the direct Coulomb interaction and where

$$U_{DA}^{ex} = -\sum_{\substack{i,j \\ \in I_D}} \sum_{\substack{R,S \\ \in I_A}} \sum_{\sigma,\sigma'} (\phi_i \phi_S | \phi_R \phi_j) \times \langle \Psi_D^* | c_{i\sigma}^\dagger \, c_{j\sigma'} | \Psi_D \rangle \, \langle \Psi_A | c_{R\sigma'}^\dagger \, c_{S\sigma} | \Psi_A^* \rangle \tag{72}$$

describes the exchange interaction which is well-known in multi-electron systems. The term U_{DA}^c in (71) encapsulates the Coulomb mechanism introduced above; in the limit that donor and acceptor are sufficiently separated such that only the leading (in case of optically allowed excitations $|\Psi_D\rangle \rightarrow |\Psi_D^*\rangle$, $|\Psi_A\rangle \rightarrow |\Psi_A^*\rangle$) dipole-dipole contributions need to be evoked, the coupling is that described originally by Förster [25]. The term U_{DA}^{ex} in (72) encapsulates the Dexter mechanism [28] also introduced above. Due to the close proximity of donor and acceptor and the involvement of the optically forbidden $2^1A_g^-$ excitation in energy transfer between lycopene and BChls in LH-II, both (71), without evoking the dipolar approximation, and (72) need to be taken into account.

The Coulomb and exchange mechanisms are illustrated in Fig. 2. In case of the Coulomb mechanism, multipole–multipole Coulomb interaction de-excites an initially excited electron on the donor molecule D and simultaneously excites an electron on the acceptor molecule A. In case of the Dexter mechanism, excitation is transferred between a donor D and an acceptor A when an excited electron, initially belonging to D, is exchanged for a non-excited electron initially belonging to A. Figure 3 depicts schematically a possible arrangement of atomic orbitals (i, j, R, S) involved in an excitation transfer. We adopt the convention that lower case letters, e.g., (i, j), denote orbitals of the donor while upper case letters, e.g., (R, S), denote orbitals of the acceptor.

Spin Tensor Properties of Electronic Couplings

The operators $\sum_{\sigma,\sigma'} c_{i\sigma}^\dagger \, c_{j\sigma} c_{R\sigma'}^\dagger \, c_{S\sigma'}$, arising in (71), and $\hat{Q}_2 = \sum_{\sigma,\sigma'} c_{i\sigma}^\dagger \, c_{j\sigma'} c_{R\sigma'}^\dagger \, c_{S\sigma}$, arising in (72), is a rank zero tensor operator for the overall (donor and acceptor) spin, but the intramolecular operators $c_{i\sigma}^\dagger \, c_{j\sigma'}$ and $c_{R\sigma'}^\dagger \, c_{S\sigma}$ can actually be expressed as sums of rank zero and rank one spin operators. Defining

$$\hat{Q}_1 = \frac{1}{2} \sum_{\sigma,\sigma} c_{i\sigma}^\dagger c_{j\sigma} \, c_{R\sigma'}^\dagger c_{S\sigma'} \, , \tag{73}$$

where the prefactor is introduced for convenience, one can express

$$\hat{Q}_1 = {}^{00}\hat{O}_j^i \, {}^{00}\hat{O}_S^R \, , \tag{74}$$

where

$${}^{00}\hat{O}_j^i = \sqrt{\frac{1}{2}} \left(c_{i\alpha}^\dagger c_{j\alpha} + c_{i\beta}^\dagger c_{j\beta} \right) \tag{75}$$

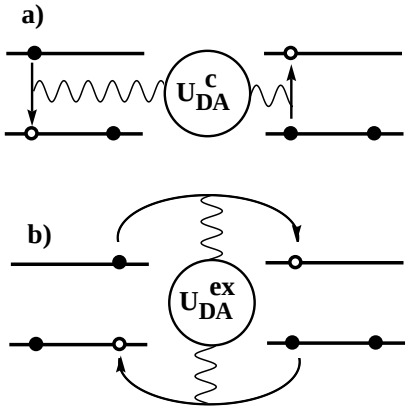

Figure 2: Schematic representation of (a) the Coulomb and (b) the Dexter mechanism of excitation transfer.

α and β denote "up" and "down" spin-$\frac{1}{2}$ states. Defining similarly

$$\hat{Q} \;=\; \frac{1}{2}\sum_{\sigma,\sigma'} \; c^{\dagger}_{i\sigma}c_{j\sigma'}\; c^{\dagger}_{R\sigma'}c_{S\sigma} \;, \tag{76}$$

one can expand

$$\begin{aligned} \hat{Q}_2 \;=\; {}^{00}\hat{O}^{i}_{j}\;{}^{00}\hat{O}^{R}_{S} \;\;&-\;\; {}^{10}\hat{O}^{i}_{j}\;{}^{10}\hat{O}^{R}_{S} \\ &+\;\; {}^{11}\hat{O}^{i}_{j}\;{}^{1-1}\hat{O}^{R}_{S} \;+\; {}^{1-1}\hat{O}^{i}_{j}\;{}^{11}\hat{O}^{R}_{S} \;. \end{aligned} \tag{77}$$

The operators introduced here, ${}^{\ell m}\hat{O}^{i}_{j}$ and ${}^{\ell m}\hat{O}^{R}_{S}$, are of rank ℓ, and are defined for $\ell = 1$ as

$$\begin{aligned} {}^{10}\hat{O}^{i}_{j} \;&=\; \sqrt{\frac{1}{2}}\left(\; c^{\dagger}_{i\alpha}c_{j\alpha} \;-\; c^{\dagger}_{i\beta}c_{j\beta}\;\right) && (78)\\ {}^{11}\hat{O}^{i}_{j} \;&=\; -\,c^{\dagger}_{i\alpha}c_{j\beta} && (79)\\ {}^{1-1}\hat{O}^{i}_{j} \;&=\; c^{\dagger}_{i\beta}c_{j\alpha}\;. && (80) \end{aligned}$$

The tensor operators ${}^{00}\hat{O}^{i}_{j}$ do not alter the spin state in the intramolecular transitions $|\Psi_D\rangle \rightarrow |\Psi^{*}_{D}\rangle$, $|\Psi_A\rangle \rightarrow |\Psi^{*}_{A}\rangle$; the tensor operators ${}^{1m}\hat{O}^{i}_{j}$ couple singlet to (1,m) triplet excitations. In case of singlet excitations the matrix elements in (72) are

$$U^{ex}_{DA} \;=\; -\,2\sum_{\substack{i,j\\ \in I_D}}\sum_{\substack{R,S\\ \in I_A}} (\phi_i\phi_S|\phi_R\phi_j)\;\langle\Psi^{*}_{D}|{}^{00}\hat{O}^{i}_{j}|\Psi_D\rangle\;\langle\Psi_A|{}^{00}\hat{O}^{R}_{S}|\Psi^{*}_{A}\rangle\;. \tag{81}$$

In case that $|\Psi_D^*\rangle$ and $|\Psi_A^*\rangle$ represent (1, +1) triplet excitations, the matrix elements are

$$U_{DA}^{ex} \;=\; 2 \sum_{\substack{i,j \\ \in I_D}} \sum_{\substack{R,S \\ \in I_A}} (\phi_i \phi_S | \phi_R \phi_j) \; \langle \Psi_D^* |^{1,1} \hat{O}_j^i | \Psi_D \rangle \; \langle \Psi_A |^{1,-1} \hat{O}_S^R | \Psi_A^* \rangle \; . \tag{82}$$

The coupling for triplet excitations (1,0) and (1,-1) yields the same numerical result as the expression above, such that only one type of triplet state needs to be considered.

We note finally that in the present notation the coupling U_{DA}^c can be expressed

$$U_{DA}^c = 2 \sum_{\substack{i,j \\ \in I_D}} \sum_{\substack{R,S \\ \in I_A}} (\phi_i \phi_j | \phi_R \phi_S) \; \langle \Psi_D^* |^{00} \hat{O}_j^i | \Psi_D \rangle \; \langle \Psi_A |^{00} \hat{O}_S^R | \Psi_A^* \rangle \tag{83}$$

Evaluation of U_{DA} in (38) then requires knowledge of the transition density matrix elements

$${}^l M_D(i,j) \;=\; \langle \Psi_D^* |^{\ell m} \hat{O}_j^i | \Psi_D \rangle \tag{84}$$

and

$${}^l M_A(R,S) \;=\; \langle \Psi_A |^{\ell m} \hat{O}_S^R | \Psi_A^* \rangle \; . \tag{85}$$

We drop the m-dependence on the left hand side since one expects identical coupling for any of the three triplet states such that the m-dependence is immaterial.

Carotenoid and Bacteriochlorophyll Electronic States

The calculation of the transition density matrix elements (84, 85) requires the description of the carotenoid and BChl electronic states involved in the excitation transfer processes. Excitation transfer between BChls and carotenoids involves exclusively π - π^* transitions.

Figure 3 depicts the conjugated π-electron system of lycopene. Lycopene has eleven conjugated double bonds, however only ten double bonds and twenty C atoms are shown in Fig. 3 and employed in our calculations. The latter choice is necessitated by the extreme computational effort to describe the π, π^*-states of lycopene. The approximation is not expected to introduce qualitative errors in the predicted lycopene $\rightarrow$ BChl excitation transfer rates since a small difference in the length of the conjugated system leaves the symmetry properties of the transition density matrix elements unchanged and introduces only small quantitative changes. We calculate transition density matrix elements employing two lycopene analogue structures, LYC_{down} and LYC_{up}. LYC_{down} consists of the twenty lycopene C atoms (belonging to the conjugated system) which are closest to B850 BChls and LYC_{up} of the twenty lycopene atoms closer to B800 BChls. All coordinates are taken from the x-ray structure of LH-II of *Rs. molischianum.*

matrix elements are based on the geometry of a symmetric BChl analogue (Fig. 3) rather than on the x-ray structure. This approximation allows one to identify the Q_y and Q_x states. (Identification of the Q_x state of the asymmetric BChl as taken from the x-ray structure is precluded since in this case these states mix strongly with higher energy excitations.)

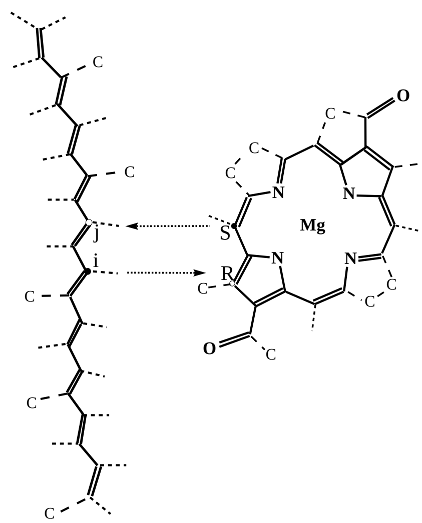

Figure 3: Schematic representation of conjugated double bonds in LYC_{down} and the bacteriochlorophyll analogue actually employed in the calculations. Representative interacting atoms i, j, R and S are indicated in the figure.

In describing the electronic states of BChl the effect of the central magnesium atom has been taken into account by adding two electrons to the conjugated system the tetrapyrrol ring.

For the required electronic states we choose a semi-empirical description as provided by the Pariser-Parr-Pople (PPP) Hamiltonian [41]

$$\begin{aligned} H \;=\; & \sum_{i<j} Z_i Z_j R_{ij} \;+\; \sum_{i,\sigma} (-I_i - \sum_{j\neq i} Z_j R_{ij}) n_{i\sigma} \\ & + \sum_{i\neq j,\sigma} t_{ij} c^+_{i\sigma} c_{j\sigma} \;+\; \frac{1}{2} \sum_{i,j,\sigma,\tilde{\sigma}} R_{ij} n_{i\sigma} n_{i\tilde{\sigma}} \end{aligned} \tag{86}$$

which involves only a minimum number of orbitals, namely those of π-type. $c^+_{i\sigma}$ and $c_{j\sigma}$ act on the mutually orthogonal atomic π-orbitals; the operator $n_{i\sigma} = c^+_{i\sigma} c_{i\sigma}$ is the corresponding number operator; R_{ij} is the effective electron-electron repulsion integral between an electron in an atomic orbital at site i and one in an orbital at site j; t_{ij} is the core integral between atoms i and j; I_i is the effective ionization potential of an orbital at site i; Z_i is the net charge of the core at atom i which was chosen as $Z_j = 1$.

The first term in (86) is constant for fixed geometries and represents the nuclear repulsion. The second term in (86) denotes the energy of an electron placed in the atomic orbital at site i, I_i is the ionization potential at atomic site i, and $-Z_j R_{ij}$ accounts for the attractive Coulomb interaction with another atomic site j. The third term in (86) describes the coupling between different atomic orbitals; it is non-vanishing for nearest neighboring orbitals only, and is evaluated according to the empirical formula [41]

$$t_{ij} \;=\; \gamma_0 \;+\; 3.21\,(r_{ij} - 1.397\text{Å})\;. \tag{87}$$

γ_0 is a constant and r_{ij} is the distance between the nuclear sites i and j. The fourth term in (86) accounts for the Coulomb interaction between the π-electrons and, following [14, 17], is expressed by the Ohno formula

$$R_{ij} \;=\; 14.397\text{eV} \times \left[\left(\frac{2 \times 14.397\text{eV}}{R_{ii} + R_{jj}} \right)^2 + \frac{r_{ij}^2}{\text{Å}^2} \right]^{-\frac{1}{2}} \tag{88}$$

The semi-empirical parameters for the PPP Hamiltonian are listed in Table 1. (SCF-CI) calculation was performed including single excited π-electron configurations for the triplet carotenoid states as well as for all bacteriochlorophyll states. Since the singlet carotenoid 2^1A_g^- state is dominated by double excited configurations [42], a basis set including both single and double excited configurations was employed for the carotenoid singlet states. The large size of this basis for a polyene with eleven double bonds, namely 7503, suggested the use of a ten bond analogue of lycopene in the calculations below.

π-electron states of polyenes obey a C_{2h} symmetry which involves 180^0 rotation about the symmetry axis (symmetry labels A, B) and the inversion at the symmetry center (symmetry labels g, u). The overall symmetry of the N electron states (here N is the number of C atoms

Table 1: Semiempirical parameters of the PPP Hamiltonian as defined in expressions (86), (87) and (88).

	$\gamma_0 = -2.43$ eV	
	$\mathrm{Z}_k = 1.0$	
	$\mathrm{r}_{k,\pm 1} = 1.35$ Å (double bonds)	
	$= 1.46$ Å (single bonds)	
Carbon (C)	Oxygen (O)	Nitrogen (N)
$\mathrm{I}_k = 11.16$ eV	$\mathrm{I}_k = 17.70$ eV	$\mathrm{I}_k = 14.12$ eV
$\mathrm{R}_{kk} = 11.13$ eV	$\mathrm{R}_{kk} = 15.23$ eV	$\mathrm{R}_{kk} = 12.34$ eV

of the conjugated system) is either A_g or B_u [15]. Besides the spatial symmetry, the PPP Hamiltonian of pure polyenes exhibits the so-called alternancy symmetry (see also appendix), according to which the π-electron states are characterized as "+" and "-" [41, 17]. Accordingly, the carotenoid states involved in our calculation are labeled $1^1\mathrm{A}_g^-$ for the ground state, $2^1\mathrm{A}_g^-$ for the optically forbidden singlet state, $1^1\mathrm{B}_u^+$ for the optically allowed singlet state and $1^3\mathrm{B}_u^+$ for the lowest energy triplet state. Singlet "+" states are reasonably well described in terms of singly excited π-electron configurations only, while singlet "−" states require single and double excited configurations for their description [42]. An inclusion of higher excitations, e.g., triple and quadruple excitations, is required to determine quantitatively the energy gaps between the electronic states of polyenes [16, 17], but are not needed to capture the essential character of the low energy polyene electronic excitations as it relates to excitation transfer rates.

Below we will employ the electronic wave functions obtained solely for the purpose of evaluating the transition density matrices (84, 85).

Transformation to Non-Orthogonal Orbitals

Coulomb and exchange couplings, U^c_{DA} (83) and U^{ex}_{DA} (81, 82), are expressed in terms of orthogonal atomic orbitals. Standard procedures of calculating Coulomb and exchange integrals, $(\phi_i\phi_j|\phi_R\phi_S)$ and $(\phi_i\phi_S|\phi_R\phi_j)$, however, involve non-orthogonal (e.g. Slater) atomic orbitals $|\tilde{\phi}_i\rangle$, related to the orthogonal orbitals $|\phi_{i'}\rangle$ as

$$|\tilde{\phi}_i\rangle \;=\; \sum_{i'} S^{\frac{1}{2}}_{i,i'}\,|\phi_{i'}\rangle\;, \tag{89}$$

or inversely

$$|\phi_{i'}\rangle \;=\; \sum_{i} S^{-\frac{1}{2}}_{i,i'}\,|\tilde{\phi}_i\rangle\;. \tag{90}$$

Here $S^{\frac{1}{2}}_{i,i'}$ ($S^{-\frac{1}{2}}_{i,i'}$) are elements of the square root (square root to the minus one) of the positive definite non-orthogonal atomic orbital overlap matrix $S_{i,i'} = S_{i',i} = \langle\tilde{\phi}_{i'}|\tilde{\phi}_i\rangle$. As suggested in

[43] we take $S_{i,i'}$ to be 1 when $i = i'$, 0.27 when atoms i and i' are joined by a chemical bond, and zero otherwise.

Employing (90) expression (83) can be rewritten in terms of non-orthogonal orbitals (here we use dummy indices i', j', R' and S' to number orthogonal atomic orbitals, and i, j, R and S for non-orthogonal orbitals)

$$\begin{aligned} U^c_{DA} &= 2 \sum_{\substack{i',j' \\ \in I_D}} \sum_{\substack{R',S' \\ \in I_A}} (\phi_{i'}\phi_{j'}|\phi_{R'}\phi_{S'})\ {}^0M_D(i',j')\ {}^0M_A(R',S') \\ &= 2 \sum_{\substack{i,j,i',j' \\ \in I_D}} \sum_{\substack{R,S,R',S' \\ \in I_A}} (\tilde{\phi}_i\tilde{\phi}_j|\tilde{\phi}_R\,\tilde{\phi}_S)\ S^{-\frac{1}{2}}_{i,i'}\ S^{-\frac{1}{2}}_{j,j'}\ S^{-\frac{1}{2}}_{R,R'}\ S^{-\frac{1}{2}}_{S,S'}\ {}^0M_D(i',j')\ {}^0M_A(R',S') \\ &= 2 \sum_{\substack{i,j \\ \in I_D}} \sum_{\substack{R,S \\ \in I_A}} (\tilde{\phi}_i\tilde{\phi}_j|\tilde{\phi}_R\tilde{\phi}_S)\ {}^0\widetilde{M}_D(i,j)\ {}^0\widetilde{M}_A(R,S)\ , \end{aligned} \tag{91}$$

where

$${}^0\widetilde{M}_D(i,j) = \sum_{\substack{i',j' \\ \in I_D}} S^{-\frac{1}{2}}_{i,i'}\ S^{-\frac{1}{2}}_{j,j'}\ {}^0M_D(i',j') \tag{92}$$

$${}^0\widetilde{M}_A(R,S) = \sum_{\substack{R',S' \\ \in I_A}} S^{-\frac{1}{2}}_{R,R'}\ S^{-\frac{1}{2}}_{S,S'}\ {}^0M_A(R',S')\ . \tag{93}$$

Similarly, expressions (81, 82) become

$$\begin{aligned} U^{ex}_{DA} &= (-1)^{l+1}\ 2 \sum_{\substack{i',j' \\ \in I_D}} \sum_{\substack{R',S' \\ \in I_A}} (\phi_{i'}\phi_{S'}|\phi_{R'}\phi_{j'})\ {}^lM_D(i',j')\ {}^lM_A(R',S') \\ &= (-1)^{l+1}\ 2 \sum_{\substack{i,j \\ \in I_D}} \sum_{\substack{R,S \\ \in I_A}} (\tilde{\phi}_i\tilde{\phi}_S|\tilde{\phi}_R\,\tilde{\phi}_j)\ {}^l\widetilde{M}_D(i,j)\ {}^l\widetilde{M}_A(R,S)\ . \end{aligned} \tag{94}$$

Expressions (91) and (94) show that the couplings can be expressed equivalently in terms of orthogonal and non-orthogonal atomic orbitals. Since we calculate the Coulomb and exchange integrals $(\tilde{\phi}_i\tilde{\phi}_j|\tilde{\phi}_R\tilde{\phi}_S)$ and $(\tilde{\phi}_i\tilde{\phi}_S|\tilde{\phi}_R\tilde{\phi}_j)$ in terms of non-orthogonal orbitals, the transition density matrix elements need to be calculated for non-orthogonal orbitals as well. These matrix elements have been evaluated according to expression (92,93) and are, for different states and pigments, shown in Figs. 4, 5, 6.

Figure 5 shows the transition density matrix elements ${}^0\widetilde{M}_A(R,S) + {}^0\ \widetilde{M}_A(S,R)$ $(R \neq S)$ and ${}^0\widetilde{M}_A(R,R)$ for the BChl $Q_x \rightarrow$ ground and $Q_y \rightarrow$ ground transitions as calculated from expression (93) for the symmetric BChl analogue (cf. Fig. 3). BChl and carotenoid triplet $\rightarrow$ ground state transitions are shown in Fig. 6.

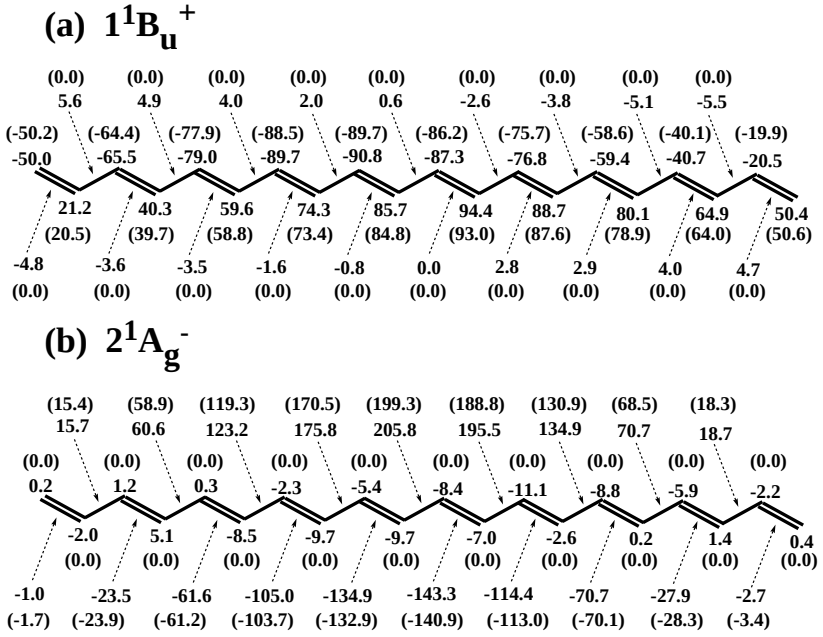

Figure 4: Transition density matrix elements ${}^0\widetilde{M}_D(i,i)$ and ${}^0\widetilde{M}_D(i,j)+{}^0\widetilde{M}_D(j,i)(i\neq j)$ in units of 10^{-3}, as defined in Eq. (92,84) for (a) the $2^1\mathrm{A}_g^- \rightarrow 1^1\mathrm{A}_g^-$ transition and (b) the $1^1\mathrm{B}_u^+ \rightarrow 1^1\mathrm{A}_g^-$ transition of lycopene (LYC_{down}). Transition density matrix elements expressed in orthogonal atomic orbitals defined in Eq. (84), i.e. ${}^0M_D(i,i)$ and ${}^0M_D(i,j)+{}^0M_D(j,i)(i\neq j)$ are shown in brackets. Numbers on atoms correspond to ${}^0\widetilde{M}_D(i,i)$, while those on bonds correspond to ${}^0\widetilde{M}_D(i,j)+{}^0\widetilde{M}_D(j,i)(i\neq j)$.

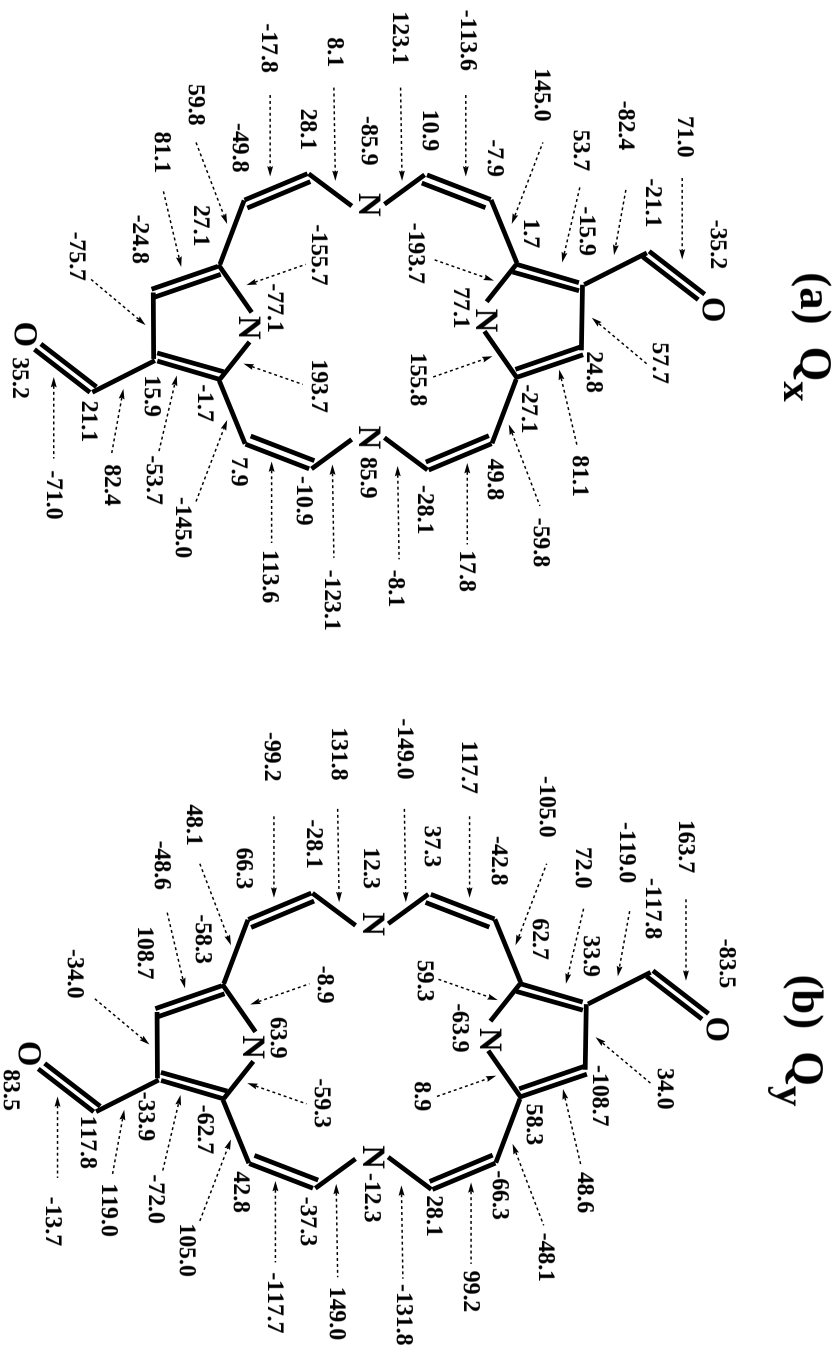

Figure 5: Transition density matrix elements ${}^0\widetilde{M}_A(R,R)$ and ${}^0\widetilde{M}_A(R,S) + {}^0\widetilde{M}_A(S,R)(R \neq S)$ in units of 10^{-3}, as defined in Eq. (92,85) for (a) the $Q_x \rightarrow$ ground transition and (b) the $Q_y \rightarrow$ ground transition of bacteriochlorophyll analogue. Numbers on atoms correspond to ${}^0\widetilde{M}_A(R,R)$, while those on bonds correspond to ${}^0\widetilde{M}_A(R,S) + {}^0\widetilde{M}_A(S,R)(R \neq S)$.

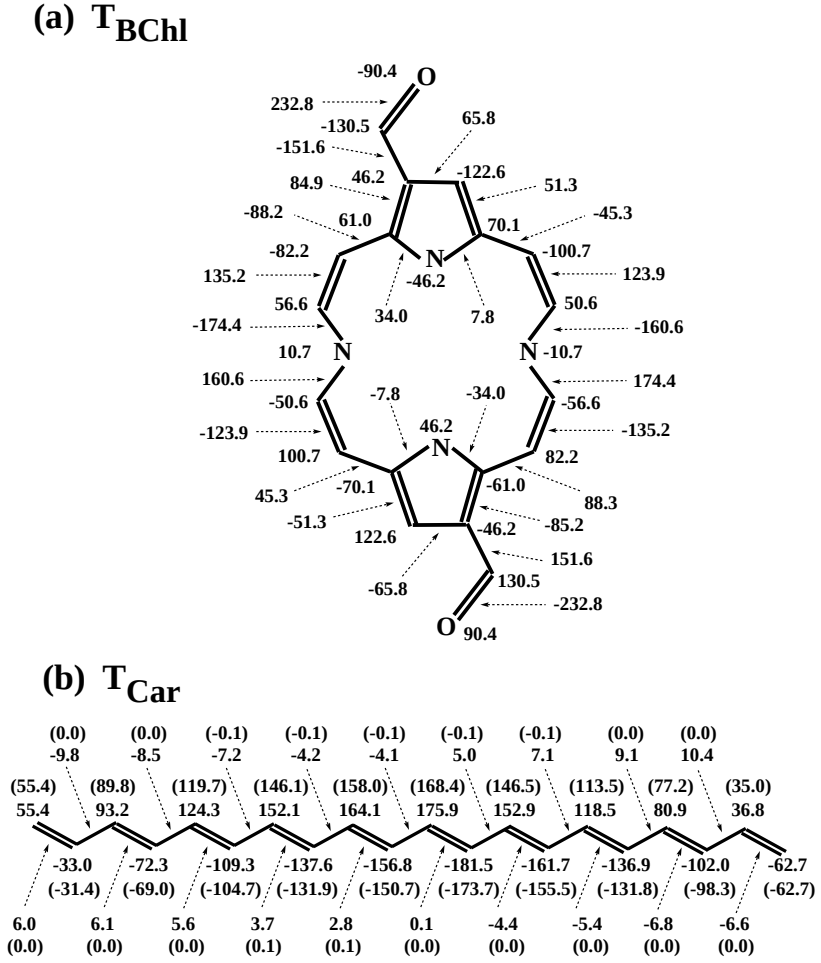

Figure 6: Transition density matrix elements (a) ${}^1\widetilde{M}_D(i,j)$, ${}^0\widetilde{M}_D(i,j) + {}^0\widetilde{M}_D(j,i)(i \neq j)$ in units of 10^{-3}, for the triplet $\rightarrow$ ground state transition of bacteriochlorophyll analogue and (b) ${}^1\widetilde{M}_A(R,S)$, ${}^0\widetilde{M}_A(R,S) + {}^0\widetilde{M}_A(S,R)(R \neq S)$ in units of 10^{-3}, for the triplet $\rightarrow$ ground state transition of lycopene (LYC_{down}). The matrix elements have been determined according to Eqs. (92, 84, 85).

Evaluation of Two-Electron Interactions

The matrix elements $(\tilde{\phi}_i\,\tilde{\phi}_j|\tilde{\phi}_R\tilde{\phi}_S)$, arising in the Coulomb term (91), can be expressed quite accurately in the Mulliken approximation

$$(\tilde{\phi}_i\tilde{\phi}_j|\tilde{\phi}_R\tilde{\phi}_S) \;=\; \frac{S_{ij}\,S_{RS}}{4}\,\Big[(\tilde{\phi}_i\tilde{\phi}_i|\tilde{\phi}_R\tilde{\phi}_R) \;+\; (\tilde{\phi}_i\tilde{\phi}_i|\tilde{\phi}_S\,\tilde{\phi}_S) \;+\; (\tilde{\phi}_j\tilde{\phi}_j|\tilde{\phi}_R\,\tilde{\phi}_R) \;+\; (\tilde{\phi}_j\tilde{\phi}_j|\tilde{\phi}_S\tilde{\phi}_S)\Big]\;. \tag{95}$$

Here S_{ij} (S_{RS}) are the elements of the atomic orbital overlap matrix as defined in the previous section. One can approximate further $(\tilde{\phi}_i\tilde{\phi}_i|\tilde{\phi}_R\tilde{\phi}_R) \;=\; e^2/R_{iR}$, *etc*, where R_{iR} is the distance between atomic centers i and R and use also $R_{iR}^{-1} \;+\; R_{iS}^{-1} \;+\; R_{jR}^{-1} \;+\; R_{jS}^{-1} \;\approx\; 4\,R_{ij,RS}^{-1}$, where $R_{ij,RS}$ is the distance between the midpoint of atoms i and j and the midpoint of atoms R and S. Accordingly, we adopt in our calculations the approximation, suggested also in [27],

$$(\tilde{\phi}_i\tilde{\phi}_j|\tilde{\phi}_R\tilde{\phi}_S) \;=\; S_{ij}\frac{e^2}{R_{ij,RS}}\,S_{RS}\;. \tag{96}$$

The exchange coupling decays exponentially with distance and, therefore, the strength of the coupling depends sensitively on the separation between donor and acceptor atoms. One must note in this respect that bridge atoms not belonging to the conjugated π-electron system, but bonded to it, can mediate electron exchange. The corresponding treatment of the two-electron interactions with exchange is described in [57].

Transition Density Matrix Elements

The atomic level structure of LH-II of *Rs. molischianum* revealed the relative arrangement of lycopenes and BChls in the protein; this permitted us to determine the Coulomb (91) and exchange (94) coupling and the associated rates of excitation transfer. Below we present the transition density matrix elements for the lycopene and BChl analogue employed in the calculations and the electronic couplings and rates for different transfer pathways.

Figure 4 shows the transition density matrix elements ${}^0\widetilde{M}_D(i,j) + {}^0\widetilde{M}_D(j,i)$ $(i \neq j)$ and ${}^0\widetilde{M}_A(i,i)$ for the carotenoid $1^1\mathrm{B}_u^+$ and $2^1\mathrm{A}_g^-$ states as calculated from expressions (92,93), i.e., employing the non-orthogonal atomic orbitals. The transition density matrix elements ${}^0M_D(i,j) + {}^0M_D(j,i)$ $(i \neq j)$ and ${}^0M_A(i,i)$ (84,85) expressed in terms of orthogonal orbitals are shown in brackets. The alternancy symmetry of polyenes is reflected in the vanishing ${}^0M_D(i,j) + {}^0M_D(j,i)$ values for the $1^1\mathrm{B}_u^+ \rightarrow 2^1\mathrm{A}_g^-$ transition for bonds $(j \;=\; i \pm 1)$ and those of the $2^1\mathrm{A}_g^- \rightarrow 1^1\mathrm{A}_g^-$ transition in the vanishing ${}^0M_D(i,i)$ values. The observed selection rules are derived in the appendix. The slight deviation of positions of lycopene C atoms from those of perfect polyenes is not destroying the alternancy symmetry, since this deviation concerns only the off-diagonal matrix elements of the PPP Hamiltonian. A change in the diagonal elements, i.e. ionization potentials of C atoms, would, however, result in disruption of alternancy symmetry.

Transition Dipole Moments

Expression (91) with the Coulomb integrals $(\tilde{\phi}_i\tilde{\phi}_j|\tilde{\phi}_R\,\tilde{\phi}_S)$ given by Eq. (96) can be expanded into a multipole series. For this purpose one starts from the well-known expansion

$$\frac{1}{|\vec{R}\,+\,\vec{r}|} \;=\; \frac{1}{R} \;-\; \frac{\vec{r}\cdot\vec{R}}{R^3} \;+\; \frac{3(\vec{r}\cdot\vec{R})^2 \;-\; r^2R^2}{2R^5} \;+\; O\left(\frac{r^3}{R^4}\right)\,. \tag{97}$$

We decompose now the distances that arise in expression (96) for the Coulomb interaction matrix elements

$$R_{ij,RS} \;=\; |\vec{R}_D \,+\, \vec{r}_{ij} \;-\; \vec{R}_A \,-\, \vec{r}_{RS}| \tag{98}$$

where $\vec{R}_D$ ($\vec{R}_A$) denote the suitably defined center of the donor (acceptor) moiety and where $\vec{r}_{ij}$ ($\vec{r}_{RS}$) are the position of the midpoints between atoms i,j (R,S) relative to the centers. One can write (98)

$$R_{ij,RS} \;=\; |\vec{R} \,+\, \vec{r}| \tag{99}$$

where

$$\vec{R} \;=\; \vec{R}_D \,-\, \vec{R}_A \qquad \vec{r} \;=\; \vec{r}_{ij} \,-\, \vec{r}_{RS} \tag{100}$$

For donors and acceptors that are distant from each other, such that the extension of donor and accpetors are much smaller than the distance between centers, holds $r/R << 1$ such that expansion (97) can be applied.

In evaluating the Coulomb coupling according to expression (93), using the multipole expansion just derived along with (96), one obtains

$$\begin{aligned} U^c_{DA} \;\approx\; U^{dd}_{DA} \;=\; & \frac{c_A\,c_D}{|\vec{R}_D-\vec{R}_A|} \;-\; \frac{\vec{R}_D-\vec{R}_A}{|\vec{R}_D-\vec{R}_A|^3}\cdot\left(c_A\,\vec{d}_D \;-\; c_D\,\vec{d}_A\right) \;+\; \frac{3}{2\,|\vec{R}_D-\vec{R}_A|^5} \;\times \\ \times\; & \left\{c_A\,\left[\vec{d}_D\cdot(\vec{R}_D-\vec{R}_A)\right]^2 \;2\,\left[\vec{d}_D\cdot(\vec{R}_D-\vec{R}_A)\right]\,\left[\vec{d}_A\cdot(\vec{R}_D-\vec{R}_A)\right] \;+\; c_D\,\left[\vec{d}_A\cdot(\vec{R}_D-\vec{R}_A)\right]^2\right\} \\ -\; & \frac{1}{2\,|\vec{R}_D-\vec{R}_A|^3}\,\left[\,(\,c_A\,|\vec{d}_D|^2) - 2\,\vec{d}_D\cdot\vec{d}_A + (\,c_D\,|\vec{d}_A|^2)\,\right] \;+\; \mathrm{O}\left(\frac{1}{|\vec{R}_D-\vec{R}_A|^4}\right)\,. \end{aligned} \tag{101}$$

Here c_D and c_A are the monopole moments of donor and acceptor defined through

$$c_D \;=\; \sqrt{2}\,e\,\sum_{i,j} S_{ij}\;\widetilde{M}_D(i,j) \tag{102}$$

$$c_A \;=\; \sqrt{2}\,e\,\sum_{R,S} S_{RS}\;\widetilde{M}_A(R,S)\,, \tag{103}$$

and $\vec{d}_D$ and $\vec{d}_A$ are the respective dipole moments

$$\vec{d}_D \;=\; \sqrt{2}\,e\,\sum_{i,j} \vec{r}_{ij}\;S_{ij}\;\widetilde{M}_D(i,j) \tag{104}$$

$$\vec{d}_A \;=\; \sqrt{2}\,e\,\sum_{R,S} \vec{r}_{RS}\;S_{RS}\;\widetilde{M}_A(R,S)\,. \tag{105}$$

Employing Eq. (92,93) one can verify

$$c_D \;=\; \sqrt{2}\, e \sum_i M_D(i,i) \tag{106}$$

and, using (75) together with $\mathbb{1} \;=\; \sum_{i,\sigma} c^\dagger_{i\sigma} c_{i\sigma}$ and the orthogonality of $|\Psi^*_D\rangle$, $|\Psi_D\rangle$, one can show that the monopole c_D vanishes. The same holds for c_A.

This property of c_D and c_A is expected and implies that the leading term of the multipole expansion (101) is

$$U^{dd}_{DA} \;=\; -\,\frac{3}{|\vec{R}_D - \vec{R}_A|^5} \times \left[\vec{d}_D \cdot (\vec{R}_D - \vec{R}_A)\right] \, \left[\vec{d}_A \cdot (\vec{R}_D - \vec{R}_A)\right] \;+\; \frac{\vec{d}_D \cdot \vec{d}_A}{|\vec{R}_D - \vec{R}_A|^3}\,. \tag{107}$$

which is indeed a dipole – dipole term.

We note that only the consistent use of non-orthogonal atomic orbitals in calculating U^c_{DA} reproduces this result; if one employs a combination of $(\tilde{\phi}_i \tilde{\phi}_j | \tilde{\phi}_R \, \tilde{\phi}_S)$ with transition density matrix elements $M_D(i,j)$ and $M_A(R,S)$ rather than $\widetilde{M}_D(i,j)$ and $\widetilde{M}_A(R,S)$, the monopole terms do not necessarily vanish and grave errors result.

In a similar fashion one can derive using Eqs. (92) and notation $\vec{r}_{ii} = \vec{r}_i$

$$\vec{d}_D \;=\; \sum_i e\, \vec{r}_i \; M_D(i,i) \tag{108}$$

which in turn is equal to the well-known expression for the transition dipole moment

$$\vec{d}_D \;=\; \langle \Psi^*_D | \sum_i e\, \vec{r}_i | \Psi_D \rangle \;, \tag{109}$$

where $\vec{r}_i$ is the position of atom i. One can derive an equivalent result for $\vec{d}_A$ as defined in (105).

The calculated transition dipole moments of the different electronic states of lycopene and BChls in LH-II *Rs. molischianum* are shown in Table 2. As expected, the $2^1\mathrm{A}^-_g$ state dipole moment vanishes within the precision limited by errors in the atomic coordinates. The calculated transition dipole moment of $1^1\mathrm{B}^+_u$ agrees well with the experimental value of 13 Debye [58]. The value of the transition dipole moment of Q_x agrees also remarkably well with the experimental value of 3.29 Debye; however, the calculated value of the transition dipole moment of Q_y exceeds the measured value of 6.13 Debye [59] by more than a factor of two.

We now revisit the dipolar coupling term in (107) and rewrite U^{dd}_{DA} as

$$U^{dd}_{DA} \;=\; \frac{\kappa}{n^2\, r^3_{DA}}\, |\vec{d}_D|\, |\vec{d}_A|, \tag{110}$$

where we have introduced the refractive index n, The orientation factor κ is defined by

$$\kappa = cos\gamma - 3cos\beta_D cos\beta_A \tag{111}$$

Table 2: Transition dipole moments in Debye for subunit one of LH-II of *Rs. molischianum*, calculated according to Eqs. (104, 105). In case of lycopene we present the results for LYC_{down} only.

Pigment (State)	d_x	d_y	d_z	$\lvert\vec{d}\rvert$
LYC ($2^1\mathrm{A}_g^-$)	-0.002	0.001	0.000	0.002
LYC ($1^1\mathrm{B}_u^+$)	2.577	10.598	-10.444	15.101
B850a (Q_y)	-13.777	-1.838	-3.771	14.402
B850a (Q_x)	0.006	-0.145	-3.383	3.386
B850b (Q_y)	12.972	4.686	-3.896	14.332
B850b (Q_x)	0.073	-0.242	-3.396	3.406
B800 (Q_y)	10.738	9.282	-2.117	14.351
B800 (Q_x)	-0.905	2.793	1.712	3.399

where γ is the angle between the two transition moments of D and A, i.e., $\vec{d}_D$ and $\vec{d}_A$; β_D is the angle between the position vector ($\vec{r}_{DA}$) and $\vec{d}_D$, and β_A is the angle between $\vec{r}_{DA}$ and $\vec{d}_A$.

Inserting the expression for the dipole-dipole coupling (111) into the rate equation (38), and identifying the spectral functions in expressions (46,47), results in the famous Förster formula for excitation transfer rate through purely dipolar coupling

$$k_{D-D} \;=\; \frac{9\ln 10\,\hbar^5\,c^4}{8\,N\,\tau_0}\;\frac{\kappa^2}{r_{DA}^6}\;\int\limits_{E=0}^{\infty} dE\;\frac{f_D(E)}{E^3}\,\frac{\varepsilon_A(E)}{E}\;. \tag{112}$$

It is Förster's achievement to realize that excitation energy transfer can be viewed formally as the combined process of emission of a photon from the donor excited state D^* and simultaneous absorption of the photon by the acceptor ground state A. Thus, he could relate the rate of excitation transfer to optical properties of donor and acceptor molecules. This correspondence is still used today, for example in determining distances between chromophores in proteins by measuring their excitation transfer rates and optical properties and calculating the corresponding distance according to Förster's formula. It should be noted, though, that the correspondence between excitation transfer and radiative processes described here is only a formal one. Excitation transfer is a radiationless process and no real photon is exchanged.

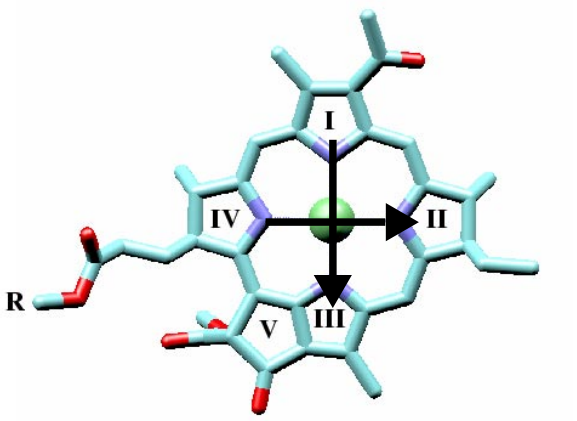

Figure 7: Structure of BChl *a*. R denotes the pyhtyl tail of BChl. The arrows indicate the transition dipole moments for the Q_y (from pyrrol ring II to IV) and the Q_x (from pyrrol ring I to III) transitions.

Electronic Excitations of Chlorophyll Aggregates

Excitations of Individual Chlorophylls

Chlorophylls are the main photosynthetic light absorbers. They consist of a porphyrin with a magnesium center. Many variants exist, with slight differences in absorption and emission properties. In purple bacteria, bacteriochlorophyll *a* (BChl) are employed and we shall describe their structure and optical properties in more detail. The chemical structure of BChl*a* is displayed in Figure 7. One can discern the characteristic structure of porphyrins, five pyrrol rings, which are labeled according to the Fisher nomenclature. In BChl*a* rings II and IV are saturated.

The absorption spectrum of BChl*a* is shown in Figure 8. One can identify four distinct excitations. The two lowest excitations at 773 and 577 nm belong to the visible Q band, which is responsible for the colorization of BChls, the two higher excitations at 391 and 358 nm belong to the Soret or B band in the ultraviolet. The lowest so-called Q_y excitation at 773 nm is characterized by a transition dipole moment along the y axis, which is defined as the axis through the two opposite, reduced pyrrol rings II and IV. The transition dipole moment axis indicates the direction in which light is absorbed when giving rise to a transition, the square of the transition dipole moment size (the oscillator strength) is proportional to the absorption intensity. The size of the transition dipole moment therefore determines optical properties of a transition. The transition at 577 nm is perpendicular to the Q_y transition and is labeled Q_x, with the x axis defined as the axis through the pyrrol rings I and III. The higher-energetic transitions are labeled B_y (391 nm) and B_x (358 nm). For the purpose of excitation transfer between BChls in photosynthesis, the Q_y excitation is of most prominent importance, because

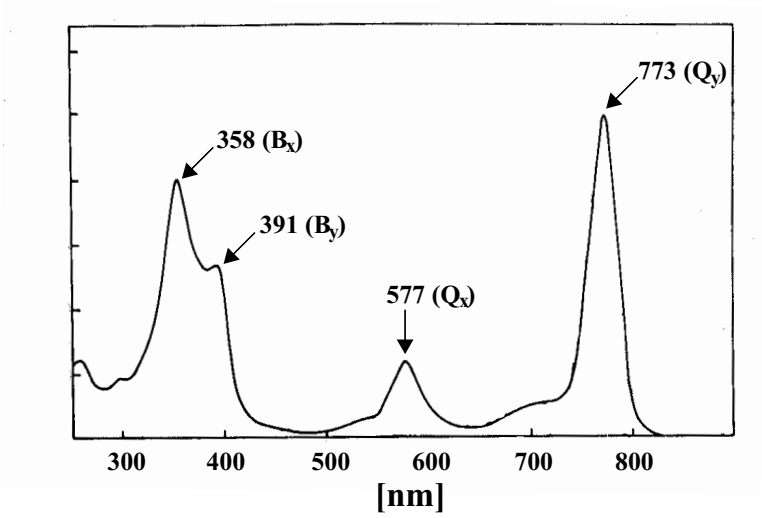

Figure 8: Absorption spectrum of monomeric BChl *a* in ether. The spectrum shows four peaks, corresponding to the Q_y transition at 773 nm, the Q_x transition at 577 nm, and the B_y and B_x transitions at 391 and 358 nm, respectively

the excitation from all higher transitions will relax within less than 1 ps into the Q_y excitation, which is therefore the donor state for practically all excitation transfers. Accessory pigments, such as carotenoids, transfer their excitation energy to BChls, in which case both the Q_x and Q_y state can serve as accepting states.

Characteristics of BChl Aggregates in Photosynthesis

The structural characteristics of the B850 BChl aggregate in LH-II from *Rhodospirillum molischianum* are depicted in Figure 9. In a first approximation, $2N$ BChls form a ring with C_{2N} symmetry. For the B850 BChl aggregate in LH-II, $2N = 16$. However, a closer inspection shows that the distances between two neighboring BChls alternates between 8.9 Å and 9.2 Å. Therefore, a more accurate description is to describe the $2N$ BChl aggregate as a system of N dimers, which obey a C_N symmetry. The transition dipole moments of the BChl Q_y excitations are oriented in the plane of and tangential to the ring of BChls. Transition dipole moments on neighboring sites show an anti-parallel orientation. The close contacts between neighboring BChls give rise to strong interactions. Due to these interactions, the stationary states of the BChl aggregates are coherent superpositions, so-called exciton states, of the lowest energy (Q_y) excitated states of individual BChls. This excitonic interaction changes the spectroscopic and excitation transfer properties of the BChl aggregates drastically when compared to those of individual BChls.

We will describe the exciton states in a circular aggregate of BChls in three descriptions

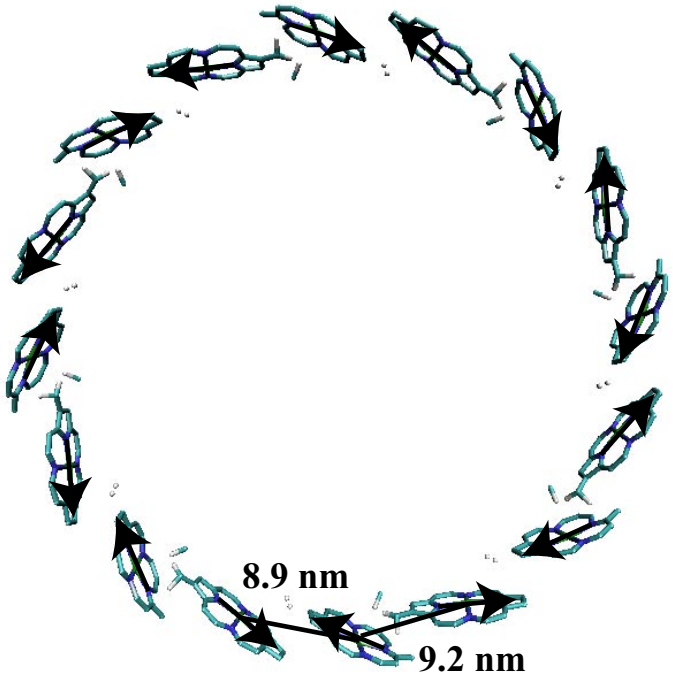

Figure 9: Schematic representation of the B850 BChl aggregate from LH-II of the purple bacterium *Rs. molischianum*. 16 BChls are arranged in a ring of 8 heterodimers. Within each dimer, the distance between BChls is 8.9 Å, between heterodimers, the distance between BChls is 9.2 Å. The transition dipole moments of the BChls, indicated as arrows are approximately tangential to the ring and show an antiparallel arrangement for a pair of neighboring BChls.

with increasing complexity. In the first two descriptions, we will consider a model in which we neglect all interactions between BChls except those between neighboring BChls. This leads to a Hamiltonian with a narrow band structure, which lends itself to easy analytical solution. In the first description, a perfect circular symmetry is assumed. The second description takes into account the dimerized structure of the BChl aggregate by differentiating between two nearest-neighbor interaction strengths. The third description includes all interactions between BChls, not only nearest-neighbor interactions. In all descriptions, it will be asumed that the relevant electronic excitations of the aggregate can be described in terms of single (intra-)BChl Q_y excitations.

Circular Aggregate with only Nearest-Neighbor Interactions

The excited states of the aggregate are described in terms of individual excitations of BChls,

$$|\alpha\rangle = |\mathrm{BChl}_1, \mathrm{BChl}_2, \ldots, \mathrm{BChl}^*_\alpha, \ldots, \mathrm{BChl}_{2N}\rangle \ . \tag{113}$$

Here, BChl_i describes the i-th BChl in the electronic ground state and BChl^*_α describes the $\alpha-$th BChl in the Q_y excited state. $2N$ is the number of BChls in the aggregate, i.e., 16 in case of the LH-II system from *Rs. molischianum*. The excited states $|n\rangle, n = 1, ..., 2N$ form an orthonormal set defining the basis of the Hamiltonian,

$$H = \begin{pmatrix} \varepsilon_0 & V & 0 & 0 & ... & 0 & 0 & V \\ V & \varepsilon_0 & V & 0 & ... & 0 & 0 & 0 \\ 0 & V & \varepsilon_0 & V & ... & 0 & 0 & 0 \\ . & . & . & . & . & . & & \\ 0 & 0 & 0 & 0 & ... & \varepsilon_0 & V & 0 \\ 0 & 0 & 0 & 0 & ... & V & \varepsilon_0 & V \\ V & 0 & 0 & 0 & ... & 0 & V & \varepsilon_0 \end{pmatrix} \tag{114}$$

Here, ε_0 defines the excitation energy of the Q_y state of an individual BChl and is commonly referred to as site energy. The parameter V accounts for the interaction between nearest neighbors. These interactions reflect the $2N$-fold symmetry of the aggregate. We now solve the eigenvalue problem

$$\hat{H}|\tilde{n}\rangle = E_n|\tilde{n}\rangle \ , \tag{115}$$

where $|\tilde{n}\rangle$ denote the eigenstates (exciton states) of the Hamiltonian, which can be expressed in terms of the basis states $|\alpha\rangle$,

$$|\tilde{n}\rangle = \sum_{\alpha=1}^{2N} c_{n\alpha}|\alpha\rangle \ . \tag{116}$$

Because of the C_{2N} symmetry of the Hamiltonian, a rotation C by an angle of $\phi = 2\pi/2N$ leaves the Hamiltonian unchanged. In other words, $\hat{H}$ and C commute with each other,

$$[H, C] = 0 \tag{117}$$

Because of $[H, C] = 0$, $C|\tilde{n}\rangle$ must also be a solution to the eigenvalue problem (115), and can therefore only differ by a constant factor λ from any eigenvector $|\tilde{n}\rangle$,

$$C|\tilde{n}\rangle = \lambda|\tilde{n}\rangle \tag{118}$$

On the other hand, C causes a relabeling of the individual sites,

$$C|\alpha\rangle = |\alpha - 1\rangle \tag{119}$$

Combining (118) and (119), and using (116) gives

$$C|\tilde{n}\rangle = \lambda \sum_{\alpha=1}^{2N} c_{n\alpha}|\alpha\rangle = \sum_{\alpha=1}^{2N} |\alpha - 1\rangle \tag{120}$$

Identifying the coefficients for equal basis vectors leads to a set of $2N$ equations for the $c_{n\alpha}$ which is closed because of the circular symmetry,

$$\begin{aligned}
\lambda c_{n1} &= c_{n2} && (121)\\
\lambda c_{n2} &= c_{n3} && (122)\\
. &\quad . && (123)\\
\lambda c_{n,2N-1} &= c_{n,2N} && (124)\\
\lambda c_{n,2N} &= c_{n1} && (125)
\end{aligned}$$

Iterative insertion leads to the condition $\lambda^{2N} = 1$, and thus

$$\lambda = e^{i\pi/N} \tag{126}$$

From (125) follows

$$c_{n\alpha} = \lambda^{\alpha} c_{n0} \tag{127}$$

with $c_{n0} = 1/\sqrt{2N}$ due to the normalization condition $\sum_\alpha c_{n\alpha}^2 = 1$. The exciton states of the circular aggregate with $2N$-fold symmetry are thus

$$|\tilde{n}\rangle = \frac{1}{\sqrt{2N}} \sum_{n=1}^{2N} \exp[in\alpha\pi/N]|\alpha\rangle \tag{128}$$

Inserting (128) into (115) leads to an equation for the expansion coefficients,

$$\varepsilon_0 c_{n\alpha} + V c_{n\,\alpha+1} + V c_{\,\alpha-1} = E_n c_{n\alpha} \tag{129}$$

from which follows with (128)

$$E_n = \varepsilon_0 + V\left[\exp[in\pi/N] + \exp[-in\pi/N]\right] \tag{130}$$

The term in square brackets can be identified as $2\cos(\pi n/N)$, resulting in the energies

$$E_n = \varepsilon_0 + 2V\cos\frac{\pi n}{N}, n = 1, 2, ..., 2N \tag{131}$$

The spectrum according to (131) consists of 2 non-degenerate levels as maximum level $E_{2N} = \varepsilon_0 + V$ and minimum level $E_N = \varepsilon_0 - V$. All other levels lie as pairs of degenerate eigenstates between these two levels.

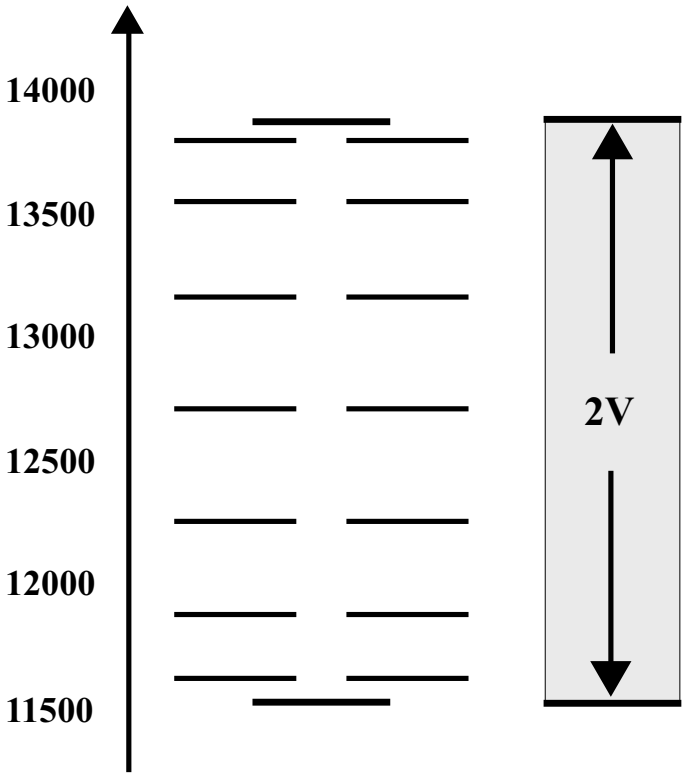

Figure 10: Spectrum of a circular aggregate of 16 BChls, using the Hamiltonian (114) which includes only nearest neighbor interactions V. The exciton states exhibit a splitting of $2V$. The exciton levels are located at $E_n = \varepsilon_0 + 2V \cos \frac{\pi n}{N}, n = 1, 2, ..., 2N$

Dimerized Aggregate with only Nearest-Neighbor Interactions

In the BChl system of LH aggregates, the distances between neighboring BChls within one heterodimer and neighboring BChls from two adjacent heterodimers vary, resulting in two different nearest neighbor interactions V_1 and V_2. Including this dimeric structure results in the $2N \times 2N$ dimensional Hamiltonian

$$H = \begin{pmatrix} \varepsilon_0 & v_1 & 0 & 0 & ... & 0 & 0 & v_2 \\ v_1 & \varepsilon_0 & v_2 & 0 & ... & 0 & 0 & 0 \\ 0 & v_2 & \varepsilon_0 & v_1 & ... & 0 & 0 & 0 \\ . & . & . & . & . & . & & \\ 0 & 0 & 0 & 0 & ... & \varepsilon_0 & v_2 & 0 \\ 0 & 0 & 0 & 0 & ... & V_2 & \varepsilon_0 & v_1 \\ v_2 & 0 & 0 & 0 & ... & 0 & v_1 & \varepsilon_0 \end{pmatrix} \tag{132}$$

Because of the dimeric structure of the interactions, the Hamiltonian (132) no longer exhibits a $2N$-fold circular symmetry, but only a N-fold symmetry. We rewrite (132) in a form that reflects the C_N symmetry with an underlying dimeric structure,

$$\hat{H} = \begin{pmatrix} H_{11} & H_{12} & 0 & 0 & 0 & 0 & 0 & H_{1N} \\ H_{21} & H_{22} & H_{23} & 0 & 0 & 0 & 0 & 0 \\ 0 & H_{32} & H_{33} & H_{34} & 0 & 0 & 0 & 0 \\ . & . & . & . & . & . & . & . \\ . & . & . & . & . & . & . & . \\ 0 & 0 & 0 & 0 & 0 & H_{N-2,N-1} & H_{N-1,N-1} & H_{N-1,N} \\ H_{N1} & 0 & 0 & 0 & 0 & 0 & H_{N,N-1} & H_{NN} \end{pmatrix} \tag{133}$$

Here, H_{jk} are 2×2 matrices, which can be identified through comparison with (132). One can identify, for example,

$$H_{11} \;=\; \begin{pmatrix} \varepsilon & V_1 \\ V_1 & \varepsilon \end{pmatrix}, \qquad H_{12} \;=\; \begin{pmatrix} 0 & 0 \\ V_2 & 0 \end{pmatrix}. \tag{134}$$

Furthermore, one can identify the symmetry properties

$$H_{j,j+1} \;=\; H_{j+m,j+m+1}\,, \quad m = 1, 2, \ldots N \tag{135}$$

due to the C_N symmetry of the aggregate and

$$H_{jk} = H_{kj}^{\dagger}\,, \tag{136}$$

where the dagger denotes the transpose, due to the symmetry of the interactions. The eigenvectors of (133) can be written

$$\widetilde{|n,\beta\rangle} \;=\; \frac{1}{\sqrt{N}} \sum_{k=1}^{N} \exp(2ikn\pi/N)\,|k,\beta\rangle, \qquad |k,\beta\rangle^T \;=\; (0 \cdots \underbrace{1}_{k^{th} position} \cdots 0)\; {v_{k\beta}}^T \tag{137}$$

where n can assume the values $n = 1, 2, \ldots N$. In this notation $v_{k\beta}$ represents a two-dimensional vector to be determined further below; β will be used later to label the two eigenvectors constructed in the corresponding two-dimensional space. We employ cyclic labels such that the index $k = N + 1$ is identified with $k = 1$, $k = N + 2$ with $k = 2$, etc. The eigenvalue problem is then stated in the form

$$\hat{H}|\widetilde{n,\beta}\rangle = E_{n,\beta}\,|\widetilde{n,\beta}\rangle\ . \tag{138}$$

Assuming orthonormality of the states $|k,\beta\rangle$ one obtains

$$\left(\sum_{k=1}^{N} H_{jk}\,\exp[2in(k-j)\pi/N]\right)\,\exp[2inj\pi/N]\,v_{n\beta}\ =\ E_{n\beta}\,\exp[2inj\pi/N]\,v_{n\beta}\ . \tag{139}$$

The reader should note that cyclic labels are employed as explained above. Here $v_{n\beta}$ is a, yet unknown, two-dimensional vector. Exploiting the symmetry property (135) one can demonstrate that the two-dimensional matrix

$$\hat{h}_n\ =\ \sum_{k=1}^{N} H_{jk}\,\exp[2in(k-j)\pi/N] \tag{140}$$

is independent of j such that one can state the eigenvalue problem (139) in the form

$$\hat{h}_n\,v_{n\beta}\ =\ E_{n\beta}\,v_{n\beta}\ . \tag{141}$$

Solution of this equation leads to the spectrum shown in Fig. 11.

One can identify two symmetric bands with N eigenstates in each band. In case of $v_1 > v_2$, for a given n the lower energy eigenvalue, labeled by $\beta = 1$, corresponds to a state in the lower band in Fig. 11 and the higher energy eigenvalue, labeled by $\beta = 2$, corresponds to a state in the upper band. The lowest energy eigenvalue in each band is obtained for $n = N$, the highest energy eigenvalue in each band for $n = 2N$, as follows immediately from the properties of the trigonometric function $\exp(2ikn\pi/N)$ in (137). For an evaluation of the energies $E_1, E_N, E_{N+1}, E_{2N}$, which represent the minima and maxima of the two bands, one needs to diagonalize the two matrices $\hat{h}_N$ and $\hat{h}_{2N}$ given by

$$\hat{h}_N\ = H_{11} - H_{12} - H_{18} = \begin{pmatrix} \varepsilon_0 & v_1 - v_2 \\ v_1 - v_2 & \varepsilon_0 \end{pmatrix} \tag{142}$$

$$\hat{h}_{2N}\ = H_{11} + H_{12} + H_{18} = \begin{pmatrix} \varepsilon_0 & v_1 + v_2 \\ v_1 + v_2 & \varepsilon_0 \end{pmatrix} \tag{143}$$

$$. \tag{144}$$

Solution of the eigenvalue problem associated with $\hat{h}_N$ and $\hat{h}_{2N}$ gives readily the eigenvalues

$$E_1\ =\ \varepsilon_0 - (v_1 + v_2) \tag{145}$$

$$E_N\ =\ \varepsilon_0 - (v_1 - v_2) \tag{146}$$

$$E_{N+1}\ =\ \varepsilon_0 + (v_1 - v_2) \tag{147}$$

$$E_{2N}\ =\ \varepsilon_0 + (v_1 + v_2) \tag{148}$$

$$. \tag{149}$$

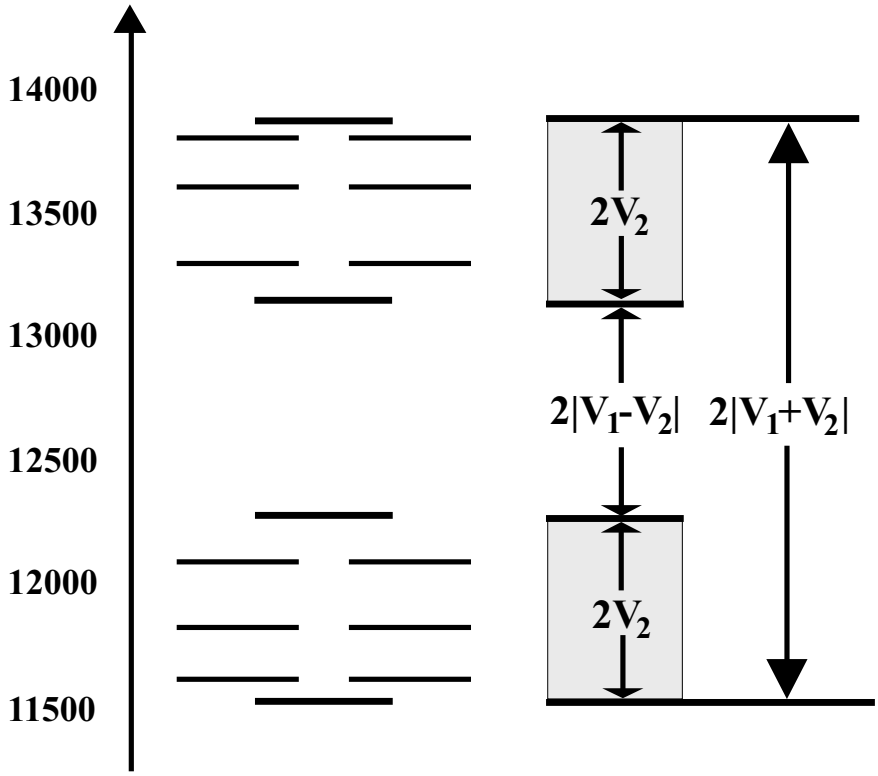

Figure 11: Spectrum of a circular aggregate of 16 BChls, with an underlying dimeric structure, reflected in two parameters v_1 and v_2 for the nearest neighbor interaction. Interactions between more distant BChls are neglected. The dimerization leads to two distinct bands, separated by a gap of width $2(v_1 - v_2)$. Each band has a width of $2v_2$, and the overall width of both bands is $2(v_1 + v_2)$.

We can thus see that the overall width of both bands displayed in Fig. 11 is $2(v_1 + v_2)$, each individual band has a width of v_2, and the gap between the two bands is $2(v_1 - v_2)$.

Effective Hamiltonian for BChl Aggregates

We now add the non-neighbor interactions to the description in the previous section. Because the distance between BChls not neighboring is > 20Å, it is reasonable to approximate the interaction by the leading term of a multipolar expansion, namely the transition dipole - transition dipole interaction term given by

$$W_{jk} \;=\; C\left(\frac{\vec{d_j}\cdot\vec{d_k}}{{r_{jk}}^3} - \frac{3(\vec{r}_{jk}\cdot\vec{d_j})\;(\vec{r}_{jk}\cdot\vec{d_k})}{{r_{jk}}^5}\right)\;, \tag{150}$$

where $\vec{d_j}$ are unit vectors describing the direction of the transition dipole moments of the ground state $\rightarrow$ Q_y state transition of the j-th BChl and $\vec{r}_{jk}$ is the vector connecting the centers of BChl j with BChl k. We consider $\vec{d_{jk}}$ to be unit vectors since the magnitudes of the transition dipole moments of BChls are treated here as unknown. The latter quantities would enter the expression for the matrix elements (150) together with a dielectric constant accounting for the optical density of the material; to repair for the missing quantities we multiply the matrix element by an *a priori* unknown constant C.

An evaluation of the dipolar coupling (150) requires knowledge of the positions of all BChls j, $j = 1, 2, \ldots 2N$ as well as knowledge of the unit vectors $\vec{d_j}$ representing the orientation of transition dipole elements. These quantities are provided through the crystal structure of LH-II. The Hamiltonian in the basis (113) for can be written

$$H = \begin{pmatrix}
\varepsilon_0 & v_1 & W_{1,3} & W_{1,4} & . & . & . & . & W_{1,2N-1} & v_2 \\
v_1 & \varepsilon_0 & v_2 & W_{2,4} & . & . & . & . & W_{2,2N-1} & W_{2,2N} \\
W_{3,1} & v_2 & \varepsilon_0 & v_1 & . & . & . & . & W_{3,2N-1} & W_{3,2N} \\
W_{4,1} & W_{4,2} & v_1 & \varepsilon_0 & . & . & . & . & . & . \\
. & . & . & . & . & & & . & . & . \\
. & . & . & . & & . & & . & . & . \\
. & . & . & . & & & . & . & . & . \\
. & . & . & . & . & . & . & \varepsilon_0 & v_2 & W_{2N-2,2N} \\
. & . & . & . & . & . & . & v_2 & \varepsilon_0 & v_1 \\
v_2 & . & . & . & . & . & . & W_{2N,2N-2} & v_1 & \varepsilon_0
\end{pmatrix}. \tag{151}$$

In order to determine the parameter C, it suffices to know a single matrix element W_{jk}. We introduce a third free parameter $v_3 = W_{13}$. Its value determines the coupling strength for all transition dipole-transition dipole matrix elements, according to

$$C \;=\; v_3\left(\frac{\vec{d_1}\cdot\vec{d_3}}{{r_{13}}^3} - \frac{3(\vec{r}_{13}\cdot\vec{d_1})\;(\vec{r}_{13}\cdot\vec{d_3})}{{r_{13}}^5}\right)^{-1}\;. \tag{152}$$

To solve the eigenvalue problem for (151), we proceed analogous to the previous section.

First, we define a Hamiltonian reflecting the dimerized structure, as

$$\hat{H} = \begin{pmatrix} \hat{H}_{11} & \hat{H}_{12} & . & . & . & . & . & \hat{H}_{18} \\ \hat{H}_{21} & \hat{H}_{22} & . & . & . & . & . & \hat{H}_{28} \\ . & . & . & . & . & . & . & . \\ . & . & . & . & . & . & . & . \\ . & . & . & . & . & . & . & . \\ . & . & . & . & . & . & . & . \\ . & . & . & . & . & . & . & . \\ \hat{H}_{81} & \hat{H}_{82} & . & . & . & . & . & \hat{H}_{88} \end{pmatrix} . \tag{153}$$

Here the $\hat{H}_{jk}$ are again 2×2 matrices which can be identified through comparison with (151). The same symmetry relations as in the previous section hold, namely

$$\hat{H}_{jk} \;=\; \hat{H}_{j+m,k+m} \;, \quad m = 1, 2, \ldots 8 \;. \tag{154}$$

and

$$\hat{H}_{jk} = \hat{H}_{kj}^{\dagger} \;. \tag{155}$$

The identity of the symmetries implies that the eigenvectors can be determined through an identical procedure as in the previous section. From (140), we obtain the matrices h_N and h_{2N}, necessary for the evaluation of the boundary state energies for the two spectral bands,

$$\hat{h}_4 \;=\; \hat{H}_{11} \,-\, \hat{H}_{12} \,+\, \hat{H}_{13} \,-\, \hat{H}_{14} \,+\, \hat{H}_{15} \,-\, \hat{H}_{16} \,+\, \hat{H}_{17} \,-\, \hat{H}_{18} \;, \tag{156}$$

$$\hat{h}_8 \;=\; \hat{H}_{11} \,+\, \hat{H}_{12} \,+\, \hat{H}_{13} \,+\, \hat{H}_{14} \,+\, \hat{H}_{15} \,+\, \hat{H}_{16} \,+\, \hat{H}_{17} \,+\, \hat{H}_{18} \;. \tag{157}$$

The matrix elements of the 2×2 Hamiltonians (156, 157) are expressed in terms of the parameters ϵ, v_1, v_2, v_3 as explained above and require a straightforward, albeit numerical, evaluation of the coupling energies (150) based on the coordinates and transition dipole moments provided through the crystal structure.

The eigenvalue problem associated with (156, 157) can be solved readily and one obtains

$$\begin{aligned} E_1 &= \varepsilon_0 + 1.942 v_3 - \sqrt{0.576 {v_3}^2 + (v_1 + v_2 - 0.638 v_3)^2} \\ E_8 &= \varepsilon_0 - 1.513 v_3 - \sqrt{0.089 {v_3}^2 + (v_1 - v_2 + 0.038 v_3)^2} \\ E_9 &= \varepsilon_0 - 1.513 v_3 + \sqrt{0.089 {v_3}^2 + (v_1 - v_2 + 0.038 v_3)^2} \\ E_{16} &= \varepsilon_0 + 1.942 v_3 + \sqrt{0.576 {v_3}^2 + (v_1 + v_2 - 0.638 v_3)^2} \end{aligned} \tag{158}$$

The resulting spectrum can be seen in Figure 12. It shows a two-band structure, with an approximate overall width of $2(v_1 + v_2)$, and an approximate gap width of $2(v_1 - v_2)$. The main effect of the non-nearest neighbor interactions is to break the symmetry between the two bands, which results in the lower band being larger than the upper band. By adjusting the parameters v_1, v_2, and v_3, one can reproduce the boundary features of any two-band spectrum of a circular BChl aggregate.

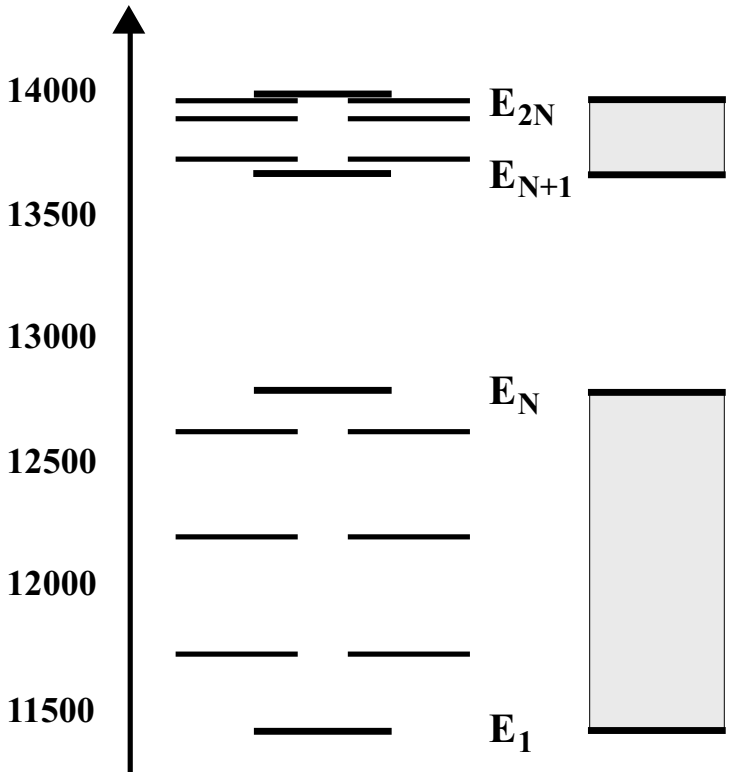

Figure 12: Spectrum of a circular aggregate of 16 BChls, with an underlying dimeric structure, reflected in two parameters v_1 and v_2 for the nearest neighbor interaction. Interactions between more distant BChls are included in a dipolar approximation with an additional parameter v_3 defining the coupling strength. The inclusion of the additional parameter v_3 breaks the symmetry between the two bands, making the lower band larger than the upper band.

Optical Properties of Circular Aggregates

A key function of the BChl aggregate in the light harvesting complexes is optical absorption. Naturally, the optical absorption characteristics of the exciton states should be characterized. Using the expansion of the exciton states in the single BChl excitation basis (116), one can express the transition dipole moment $\vec{f}_n$ associated with the the exciton state $|\tilde{n}\rangle$ as

$$\vec{f}_n = \sum_{\alpha=1}^{N} c_{n\alpha} \vec{d}_\alpha \tag{159}$$

where $\vec{d}_\alpha$ is the transition dipole moment for the Q_y transition of BChl α. The dipole strength associated with the transition to the state $|\tilde{n}\rangle$ is $|\vec{f}_n|^2$.

The exciton states can be assumed to be orthonormal, i.e.,

$$\langle \tilde{n}|\tilde{m}\rangle \;=\; \delta_{nm} \; . \tag{160}$$

An orthonormality relation also holds for the single BChl excitations,

$$\langle \alpha|\alpha'\rangle \;=\; \delta_{\alpha\alpha'} \; . \tag{161}$$

From properties (160, 161) follows

$$\sum_{n=1}^{2N} C^{\dagger}_{n\alpha} \, C_{n\alpha'} \;=\; \delta_{\alpha\alpha'} \; , \tag{162}$$

where the dagger denotes the complex conjugate. One can derive then readily the oscillator strength sum rule

$$\sum_{n=1}^{2N} |\vec{f}_n|^2 \;=\; \sum_{\alpha=1}^{2N} |\vec{D}_\alpha|^2 \;=\; 2N \, S_y \; . \tag{163}$$

where the second equality follows from the fact that all BChls carry identical dipole strengths $|\vec{D}_\alpha|^2 \;=\; S_y$. The sum rule (163) implies that the sum of the oscillator strengths of all exciton states $|\tilde{n}\rangle$ is equal to $2N$ times the oscillator strength of the Q_y transition of the individual BChls. This rule applies, irrespective of the circular symmetry of the system. In case of an uncoupled system each BChl carries the same oscillator strength; however, in the case of coupled BChls, the resulting exciton states do not share the oscillator strength equally.

For the case of a system of $2N$ BChls in C_{2N} symmetrical arrangement, the transition dipole moments associated with the excitons are

$$\langle \text{ground}|\vec{\mathcal{D}}|\tilde{\alpha}\rangle \;=\; \frac{1}{\sqrt{2N}} \sum_{n=1}^{2N} e^{in\alpha\pi/N} \, \vec{d}_n \tag{164}$$

Here $\vec{d}_n$ denotes the transition dipole moments of the individual BChls which are oriented in within the plane of the membrane as shown in Figure 9 and can be represented as

$$\vec{D}_n \;=\; D_0 \begin{pmatrix} \cos\phi_n \\ \sin\phi_n \\ 0 \end{pmatrix} \; , \qquad \phi_n \;=\; \frac{\pi n(N+1)}{N} \; , \quad n \;=\; 1, 2, \ldots 2N \; . \tag{165}$$

From (164) one obtains for the dipole strength of the ground state $\rightarrow$ $|\tilde{\alpha}\rangle$ transition

$$|\langle \text{ground}|\vec{\mathcal{D}}|\tilde{\alpha}\rangle vert^2 \;=\; N\, D_0^2\,(\,\delta_{\alpha,-N+1} \;+\; \delta_{\alpha,N-1}\,)\;. \tag{166}$$

Only two excitons with degenerate energies

$$\epsilon_{\pm} \;=\; \varepsilon_0 \;-\; 2\,V\,\cos\frac{\pi}{N} \tag{167}$$

carry oscillator strength. These are actually the 2nd and 3rd lowest electronic excitations of the aggregate.

Couplings to Excitonic States

Electronic excitations in the ring of LH-II's sixteen B850 BChls are strongly coupled because of the close proximity of neighboring units (Mg-Mg distance 8.9 or 9.2 Å). Due to this strong coupling, electronic singlet excitations form completely delocalized excitons in the absence of disorder [51]. In our calculations we employ an effective Hamiltonian describing excitons delocalized over the entire ring. This has to be considered an approximation since static and dynamic disorder disrupts the coherency [52]. The suitability of such approximation is further analyzed in the discussion.

An effective Hamiltonian, limited to the Q_y excitations of the individual BChls, has been constructed and described in [12]. The basis set defining the matrix representation of the effective Hamiltonian contains the elements

$$||\alpha\rangle\rangle \;=\; \psi_1(\mathrm{g})\cdots\psi_{\alpha-1}(\mathrm{g})\psi_\alpha(\mathrm{Q}_y)\psi_{\alpha+1}(\mathrm{g})\cdots\psi_{2N}(\mathrm{g})\;. \tag{168}$$

Here, $\psi_j(\mathrm{g})$ describes the j-th BChl in the electronic ground state and $\psi_\alpha(\mathrm{Q}_y)$ describes the α-th BChl in the Q_y excited state; $2N$ is the number of BChls in the aggregate, i.e., 16 in case of the B850 system of *Rs. molischianum*. Due to pair-wise dimerization of BChls in LH-II, the spectrum of the Hamiltonian displays only an N-fold symmetry, featuring four non-degenerate states (E_1 = 11482 cm^{-1}, E_8 = 12863 cm^{-1}, E_9 = 13715 cm^{-1}, E_{16} = 14046 cm^{-1}) and twelve pairwise degenerate states ($E_{2,3}$ = 11765 cm^{-1}, $E_{4,5}$ = 12250 cm^{-1}, $E_{6,7}$ = 12676 cm^{-1}, $E_{10,11}$ = 13794 cm^{-1}, $E_{12,13}$ = 13922 cm^{-1}, $E_{14,15}$ = 14012 cm^{-1}) [12]. The corresponding eigenstates of this Hamiltonian, the so-called excitonic states (excitons), are represented generically

$$||n\rangle \;=\; \sum_{\alpha=1}^{2N} C_{n\alpha}\,||\alpha\rangle\rangle\;. \tag{169}$$

Here, $C_{n\alpha}$ are the expansion coefficients as characterized in [12].

Singlet excitation transferred from lycopene (or B800 BChl) towards the B850 BChls is not absorbed into electronic excitations of individual BChls, but into excitonic states. The

Coulomb coupling between the carotenoid state $|\Psi_{car}\rangle$ and the excitonic state $||n\rangle$ is

$$U^c_{DA}(n) \;=\; \sum_\alpha C_{n\alpha} \sum_{i,j,R,S} S_{ij} \frac{e^2}{R_{ijRS}(\alpha)} S_{RS} \times \langle \Psi^*_D| \sum_\sigma c^\dagger_{i\sigma}\, c_{j\sigma} |\Psi_D\rangle \, \langle\langle \alpha|| \sum_\sigma c^\dagger_{R\sigma}\, c_{S\sigma} ||0\rangle \,, \tag{170}$$

where $||0\rangle$ represents the electronic ground state of the BChl aggregate.

In case of energetically degenerate exciton states (m_1, m_2), excitation can be absorbed into any linear combination $\cos\gamma\, ||m_1\rangle + \sin\gamma\, ||m_2\rangle$ of these two states. We choose that combination which renders the resulting coupling

$$U^c_{DA}(m_1, m_2) \;=\; \cos\gamma\, U^c_{DA}(m_1) \;+\; \sin\gamma\, U^c_{DA}(m_2) \tag{171}$$

maximal. This combination is defined through the angle γ specified through

$$\tan 2\gamma \;=\; \frac{2\, U^c_{DA}(m_1)\, U^c_{DA}(m_2)}{U^c_{DA}(m_1)^2 \;-\; U^c_{DA}(m_2)^2} \,. \tag{172}$$

In the following we introduce a single index m to enumerate the degenerate states m_1 and m_2 and replace $U_{DA}(m_1, m_2)$ by $U^c_{DA}(m)$. In this manner we will relabel the states such that only one index labels a linear combination (with γ as defined by (172)) of two degenerate states, i.e., we will count subsequently only states with different energy.

The rate of excitation transfer into excitonic state $||n\rangle$ is

$$k_{DA}(n) \;=\; \frac{2\,\pi}{\hbar} \;|U_{DA}(n)|^2 \int S_D(E)\; S_{A,n}(E)\; dE \,, \tag{173}$$

while the total excitation transfer rate is a sum

$$k_{DA} \;=\; \sum_n k_{DA}(n) \,. \tag{174}$$

The Effect of Disorder

The described electronic structure of LH-II assumes perfect circular symmetry and neglects any kind of structural or thermal disorder. The disorder broadens the absorption spectrum and shortens the effective exciton delocalization length. The disorder can be classified into two types; the dynamic disorder - a consequence of thermal motion of the protein and the chlorophylls, and the static disorder - a consequence of structural inhomogeneities of the protein which induce differences in the local excitation energies of the chlorophylls.

Static Disorder

The effect of the static disorder on the energy levels and oscillator strengths of an absorbing molecule can be studied with time-independent Hamiltonians. In the following we consider the ring of B850 chlorophylls in LH-II.

At first we will assume that the the off-diagonal elements of the effective Hamiltonian are unchanged and obey the C_8 symmetry, but that the diagonal matrix elements are distributed according to a random distribution

$$\hat{H}_{rand} = \begin{pmatrix} \epsilon_1 & v_1 & & & & & & v_2 \\ v_1 & \epsilon_2 & & & & & & \\ & & . & & W_{ij} & & & \\ & & & . & & & & \\ & & & & . & & & \\ & & W_{ij} & & & . & & \\ & & & & & & & \\ v_2 & & & & & & v_1 & \epsilon_N \end{pmatrix} . \tag{175}$$

Here, each of the sixteen diagonal energies $(\epsilon_1, \epsilon_2, \ldots, \epsilon_{16})$ is chosen according to the Gaussian distribution

$$p(\epsilon_\alpha) \; = \; \frac{1}{\sqrt{2\pi}\sigma} \exp\left[-(\epsilon_\alpha \, - \, \epsilon)^2/2\sigma^2\right] \; . \tag{176}$$

We generated, by means of a random number generator, an ensemble of 1,000 random Hamiltonians H_{rand}. Each of the random Hamiltonians was then diagonalized and average excitation energies as well as the average oscillator strengths for all exciton states were determined. We carried out such calculation for σ-values ranging from 0 to 1,500 cm^{-1} in steps of 5 cm^{-1}. The resulting energies and oscillator strength are provided in Fig. 13.

Figure 13a shows a splitting of the degenerate energy levels (e.g., E_2, E_3) with increasing σ, and a widening of the exciton bands. Most interesting is the redistribution of oscillator strength among the excitonic states with increasing diagonal disorder shown in Fig. 13b: the allowed states of energy E_2, E_3 lose oscillator strength, a major part of which shifts to the lowest energy exciton state. The oscillator strengths of the strongly allowed exciton states can be considered a qualitative measure of the delocalization of the exciton states in LH-II.

Hole-burning spectroscopy [72] has provided estimates for the inhomogeneous broadening of the B850 exciton system in LH-II; LH-II of *Rb. sphaeroides* exhibits a width of 60 cm^{-1}.

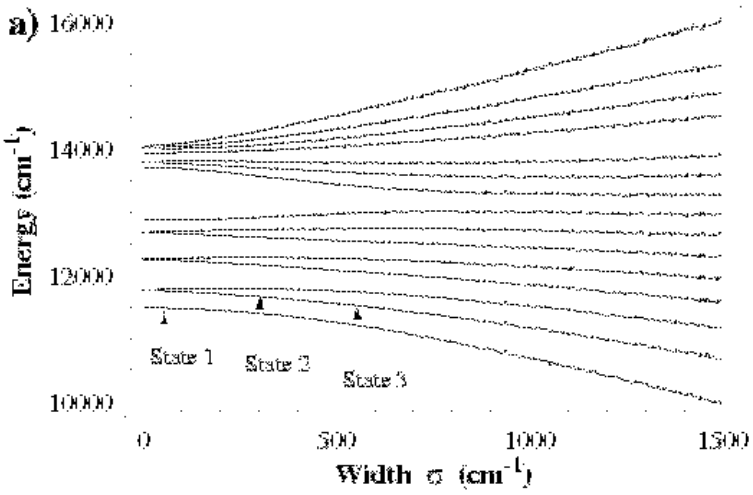

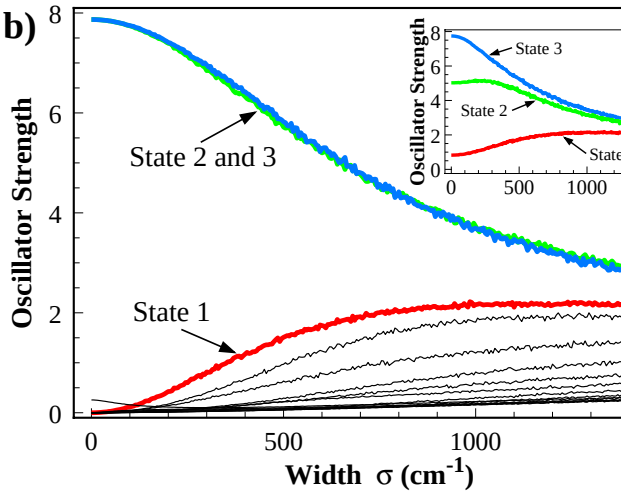

Figure 13: (a) Energy levels of the aggregate of the sixteen B850 chlorophylls in LH-II with diagonal disorder. The diagonal elements of the Hamiltonian are distributed according to a Gaussian distribution with varying width σ. Energies shown are averaged over a sample of 1,000 aggregates for each σ-value. (b) Dipole Strength (in units of dipole strength of individual chlorophyll) of the excitonic states corresponding to the energy levels in (a) for the same average over 1,000 aggregates. The oscillator strength of excitons at energies E_1, E_2, E_3 are highlighted.

According to the exchange narrowing phenomenon [73], the widths of the absorption band of a tightly coupled chlorophyll aggregate is narrowed compared to the absorption bandwidth of an individual chlorophyll. For a circular chlorophyll aggregate, the narrowing factor scales as $\sqrt{N}$, where N denotes the symmetry of the aggregate. In LH-II of *Rs. molischianum* $N = 8$, and the scaling factor assumes the value of 2.8. Assuming for the exciton bandwidth a value of 60 cm^{-1} [72] results in a value of a diagonal disorder of $\sigma = 170$ cm^{-1}.

To verify computationally the motional narrowing in LH-II we have determined the spectrum of the disordered chlorophyll aggregate for a disorder characterized through $\sigma = 170$ cm^{-1}. We considered an ensemble of 5,000 aggregates with randomly selected diagonal matrix elements in the effective Hamiltonian. The energies and oscillator strengths of all exciton states were evaluated and collected into bins of width 5 cm^{-1} along the energy axis. Figure 14 shows the resulting average spectrum of nearly Gaussian shape with a width of $\Gamma = 60$ cm^{-1}. As a reference the spectrum for a completely ordered aggregate (all diagonal elements ϵ_α equal 13,059 cm^{-1}) is also shown as well as the distribution of ϵ_α. One can recognize that the spectrum of the ensemble is narrowed relative to the distribution of ϵ_α by a factor of 2.8, in agreement with theoretical predictions.

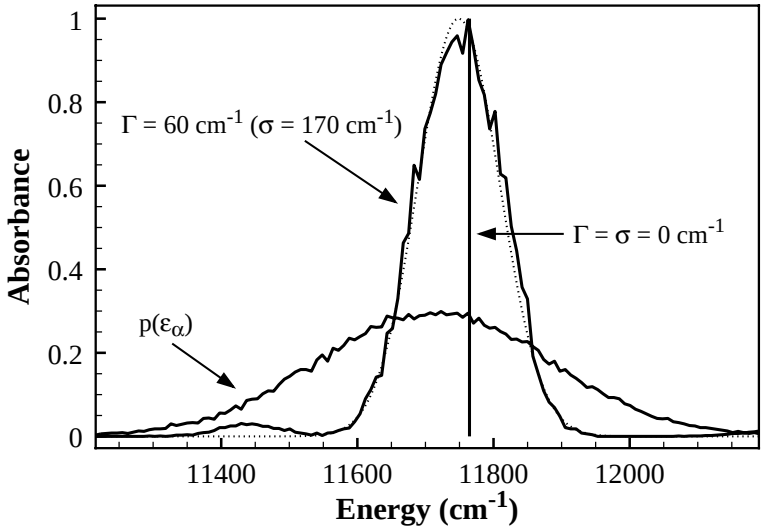

Figure 14: Absorbance of a disordered aggregate of B850 chlorophylls of LH-II. The system corresponds to those in Fig. 13 for $\sigma = 170$ cm^{-1}, albeit with a sample size of 5,000. The construction of the absorbance shown is explained in the text. The calculated absorbance is well approximated by a Gaussian with the width of 60 cm^{-1} (dotted line). The figure presents also the absorbance for $\sigma = 0$ (single stick) as well as the distribution $p(\epsilon_\alpha)$ of ϵ_α - values assumed.

As judged from the results in Fig. 13, a diagonal disorder of $\sigma = 170$ cm^{-1} produces a small effect on the dipole strengths of the excitons states in the LH-II B850 chlorophyll aggregate; the dipole strengths of states of energy E_1 and $E_{2,3}$ are about 0.3 and 7.6, respectively (in units of

dipole strength of individual chlorophyll). This implies that disorder corresponding to σ-values of about 170 cm^{-1} does not affect significantly the characteristics of the exciton states relevant for light absorption and for conservation of light energy in the lowest exciton state.

Dynamic Disorder

To understand the effect of the dynamic disorder on the broadening of the spectrum and on the excitonic states, the magnitude and timescales of the spatial fluctuations of BChls and its protein surrounding need to be determined. This has been achieved through a molecular dynamics simulation of LH-II in its natural membrane-water environment. The simulated system, consisting of about 85,000 atoms, was equilibrated for 2 ns using the molecular dynamics program NAMD [74] with periodic boundary, full electrostatics, and constant pressure and temperature conditions. After the equilibration, the snapshots of the simulation were taken every 5 fs during a 30 ps period yielding a trajectory of atomic positions of BChls and the rest of the simulated system. The atomic position of atom α at snapshot t_k will be denoted as $\vec{r}_\alpha(t_k)$.

Based on the atomic positions emerging from the molecular dynamics trajectory, time dependent exciton Hamiltonian can be constructed

$$\hat{H}(t_k) = \begin{pmatrix} \epsilon_1(t_k) & v_1(t_k) & & & & & v_2(t_k) \\ v_1(t_k) & \epsilon_2(t_k) & & & & & \\ & & . & & W_{ij}(t_k) & & \\ & & & . & & & \\ & & & & . & & \\ & & W_{ij}(t_k) & & & . & \\ v_2(t_k) & & & & & v_1(t_k) & \epsilon_N(t_k) \end{pmatrix} . \tag{177}$$

The matrix elements of the effective Hamiltonian $H_{ij}(t_k)$ can easily be determined for every snapshot of the simulation; the positions of the N-atom of pyrrole I and the N-atom of pyrrole III of BChl determine the orientation of the Q_y transition dipole moment; the magnitude of the Q_y transition dipole moment is assumed to be fixed; the values of the dipole - induced dipole matrix elements of the effective Hamiltonian $W_{i,j}(t_k)$ can thus be determined for every snapshot of the simulation

$$W_{ij}(t_k) \;=\; C \left(\frac{\vec{d}_i(t_k) \cdot \vec{d}_j(t_k)}{r_{ij}(t_k)^3} - \frac{3(\vec{r}_{ij}(t_k) \cdot \vec{d}_i(t_k))\;(\vec{r}_{ij}(t_k) \cdot \vec{d}_j(t_k))}{r_{ij}(t_k)^5} \right) . \tag{178}$$

The fluctuations of the matrix elements v_1 and v_2 during the trajectory will, for the moment, be assumed to equal the fluctuations of the dipole - induced dipole couplings for the respective BChls, e.g.,

$$v_1(t_k) \equiv H_{12}(t_k) \cong v_1(t_0) + W_{12}(t_k) - W_{12}(t_0) \; . \tag{179}$$

The fluctuations of the diagonal matrix elements $(\epsilon_1(t_k), \epsilon_2(t_k), \ldots, \epsilon_{16}(t_k))$, i.e., of the BChl Q_y excitation energies, will be determined with a quantum chemistry program *Gaussian 98* [75]. Based on the coordinates of BChl from molecular dynamics trajectory, $\vec{r}_\alpha(t_k), \alpha \in \text{BChl}_i$, and using a 3-21G basis set with an *ab initio* level of theory, the program yields the Q_y excitation energies $\epsilon_i(t_k)$. Furthermore, we calculate these energies including the charge distribution of the protein atoms, which are treated by the program *Gaussian 98* as simple background charges. The coordinates and charges of the protein are, for every snapshot, obtained from the molecular dynamics trajectory file.

Ones all of the matrix elements of the effective Hamiltonian are known for every snapshot of the trajectory $H_{i,j}(t_k)$, the Hamiltonian $\hat{H}(t_k)$ can be diagonalized, and excitation energies $E_n(t_k)$, and oscillator strengths $\vec{f}_n(t_k)$ determined. Based on this information, the absorption spectrum, as well as exciton delocalization length can, in principle, be calculated. However, at this moment a theory to determine the absorption spectrum of an aggregate of sixteen tightly coupled has not been developed. On the other hand, the existing theory to calculate the exciton delocalization length for this aggregate has not been connected with the molecular dynamics data. In the following two chapters we will briefly report on the theory to calculate absorption spectrum of a single BChl from molecular dynamics/quantum chemistry data, as well as on the theory to determine exciton delocalization length via the path integral method.

Calculation of Optical Properties of Solvated Bacteriochlorophyll

The authors in [76] have calculated absorption spectrum of BChl in methanol using a combined quantum mechanical/molecular dynamics method. Similarly to what was described above, through a molecular dynamics simulation of BChl in methanol they generated a trajectory of BChl and solvent conformations. For each snapshot of the trajectory they determined BChl excitation energies with *ab initio* method, taking into account the background charge distributions of the solvent. This combined molecular dynamics/quantum chemistry calculations yielded the fluctuations of the energy gap $\delta\omega_{eg}(t)$. The linear optical response function $R(t)$ was approximated as

$$R(t) \;=\; exp(-g(t)), \tag{180}$$

where $g(t)$ is the line-broadening function

$$g(t) \;=\; \Delta^2 \int_0^t d\tau_1 \int_0^{\tau_1} M(\tau_2)\, d\tau_2 \tag{181}$$

and $M(\tau_2)$ is the autocorrelation function of the fluctuations of the energy gap $\delta\omega_{eg}(t)$

$$M(t) \;=\; \frac{1}{\Delta^2} \int_{-\infty}^{+\infty} \delta\omega_{eg}(t+\tau)\delta\omega_{eg}(\tau)d\tau \;. \tag{182}$$

Δ is the root mean square deviation of the fluctuations of the energy gap.

Absorption spectrum can be calculated directly from the optical response function as

$$\sigma(\omega) \;=\; Re[\int_0^t R(t)\, exp[i\,(\omega \,-\, \omega_{eg})\, t]] \;. \tag{183}$$

The calculated absorption spectrum agrees well with the experimentally measured spectrum, as shown in Fig. 15 [76]. Additional information about the dynamics of the system can be obtained

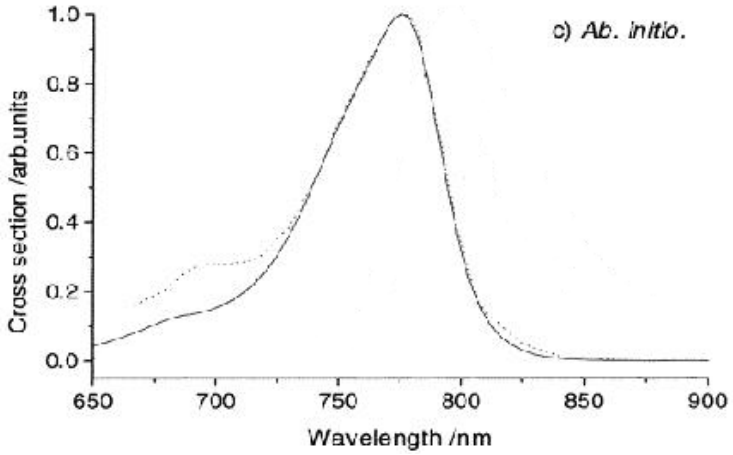

Figure 15: Obtical absorption spectrum of BChl in methanol; experimental spectrum (dotted) and calculated spectrum (solid) [76].

by comparison of the timescales of the optical linear response function with the correlation function of the fluctuating energy gap. This function is shown in Fig. 16. The duration of the amplitude of the optical response function gives the time taken for an electronic transition to occur. The linear response function calculated for BChl in methanol is shown in Fig. 17. If the energy gap correlation function decays more quickly than the amplitude of the optical response function, the optical profile is considered to be homogeneously broadened. On the other hand, if the energy gap correlation function decays more slowly than the amplitude of the optical response function, the optical profile is considered to be inhomogeneously broadened. Such is, e.g., the broadening by the static disorder. Comparison of Figures 16 and 17 indicates that the absorption profile of BChl in methanol is largely homogeneously broadened.

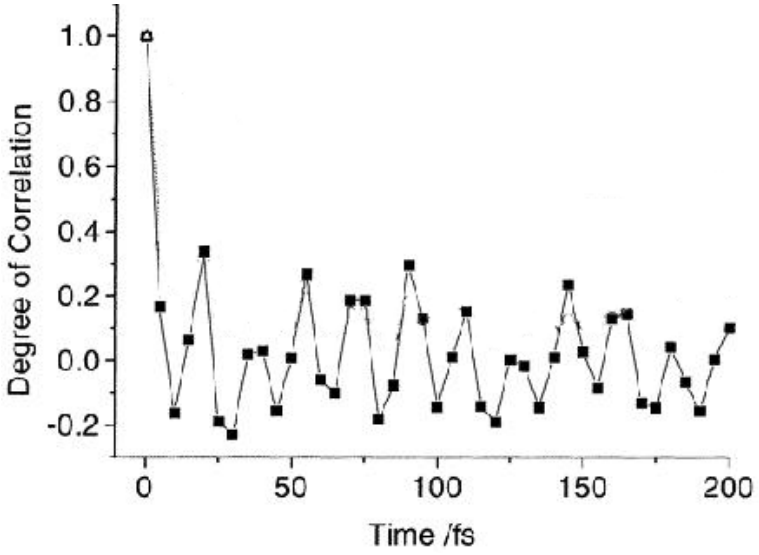

Figure 16: Energy gap correlation function [76].

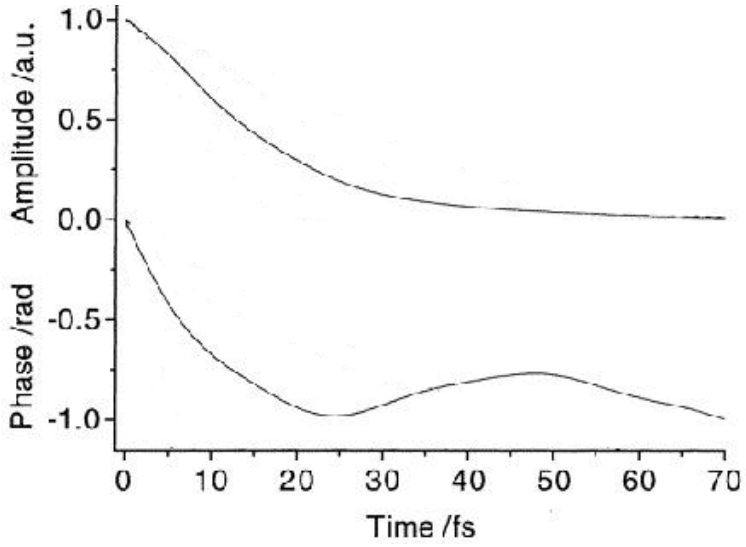

Figure 17: The linear response function calculated for BChl in methanol [76].

Random Matrix Theory of Spectral Fluctuations

As explained in the previous lectures, the effective hamiltonian for a light-harvesting complex can be put into the following form:

$$\begin{aligned} H &= H_0 + W, \\ H_0 &= \begin{pmatrix} \epsilon & v_1 & 0 & \cdots & 0 & v_2 \\ v_1 & \epsilon & v_2 & \cdots & 0 & 0 \\ 0 & v_2 & \epsilon & \cdots & 0 & 0 \\ \cdots & \cdots & \cdots & \cdots & \cdots & \cdots \\ v_2 & 0 & 0 & \cdots & v_1 & \epsilon \end{pmatrix}, \end{aligned} \tag{184}$$

where H_0 contains the excitation energies, ϵ, and nearest neighbor interactions, v_1 and v_2. Here H has dimensions $2N \times 2N$ where N is the number of chromophore pairs. $W_{ij} = W_{ji}$ is the induced dipole induced dipole interaction between chromophores i and j. The physical values for the constants that determine the hamiltonian are

$$\begin{aligned} \epsilon &= 13362\text{cm}^{-1} \\ v_1 &= 806\text{cm}^{-1} \\ v_2 &= 377\text{cm}^{-1} \end{aligned}$$

and the typical W_{ij} is smaller than roughly half the size of v_2.

Since no physical copies of the system are identical, the hamiltonian described above should be studied in a statistical setting. Furthermore, as a result of dynamic effects, the chromophore location and orientation changes in time, changing the W_{ij} as a result. It can be argued that the fluctuations in W_{ij} are so significant that it can be treated as a random component. Hence we are led to study a system consisting of a *deterministic* (i.e. non-changing) part, H_0, and a *random* (i.e. fluctuating) part, W. We will consider W to be drawn from a probability distribution $P(W)$, which will be specified later.

Physical characteristics of the system are given by its energy spectrum. More specifically we will be interested in the *spectral density* (i.e. the density of the eigenvalues in the energy axis), which can be written as

$$\rho(\lambda) = \left\langle \sum_i \delta(\lambda - \lambda_i) \right\rangle \tag{185}$$

where the brackets denote an ensemble average over the set of random matrices, W, with respect to the probability density, $P(W)$. The spectral density, $\rho(\lambda)d\lambda$, gives the probability for finding an eigenvalue of H near λ as averaged over all W.

This kind of study falls under the domain of *random matrix theory* [77], which studies spectral properties of ensembles of hamiltonians. In particular, there are analytical tools in random matrix theory, which enables one to study the spectrum of deterministic-plus-random system, from the knowledge of its parts.

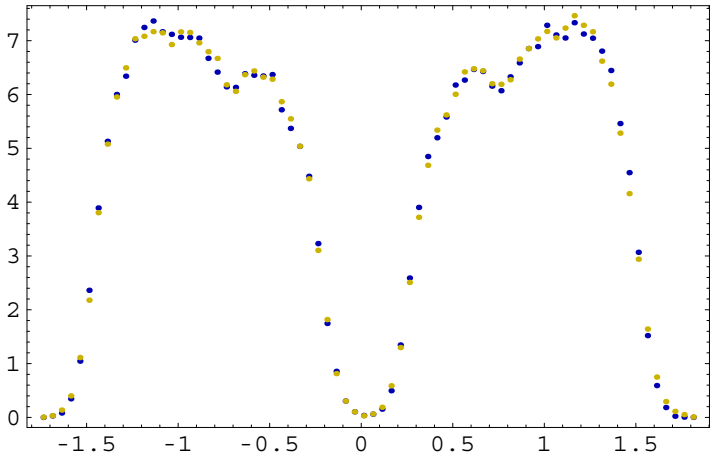

Figure 18: Universality in random matrix theory: the two curves denote the spectral densities obtained numerically for $2N = 16$ where the random part of the hamiltonian is a real symmetric matrix. The matrix elements are drawn from a flat distribution for the blue curve and from a gaussian distribution for the yellow curve. The variances of the two distributions are equal. The spectral density is centered around ϵ and rescaled for convenience.

In the case where the random part, W, vanishes the spectrum of H reduces to that of H_0, which can be shown to be given by

$$\gamma_{\pm i} = \epsilon \pm \sqrt{v_1^2 + v_2^2 + 2v_1 v_2 \cos\left(\frac{2\pi i}{N}\right)}\ ; \quad i = 1, \ldots, N. \tag{186}$$

It can be observed that, the spectrum splits in to two 'bands' which are split apart by a distance given by $v_1 - v_2$ and all energy levels, except for those defining the band boundaries, are doubly degenerate. This degeneracy may be viewed as a consequence of the C_N symmetry of the hamiltonian.

Now if we 'turn on' the random part, W, it shall be expected that the locations of the eigenvalues of H are 'smeared'. To put it more precisely, the average spectral density defined in (185) now becomes a smooth function instead of a sum over delta functions. The average spectral density can be obtained numerically, by diagonalizing a set of matrices $H_0 + W$ with W drawn randomly from the distribution $P(W)$ and making a histogram of the eigenvalues obtained this way.

Figure 18 gives the result of just such a study. One important issue is the choice of the probability density, $P(W)$. It is almost customary to choose a gaussian

$$\begin{aligned} P(W) &= N_W \exp\left(-\frac{1}{2\nu^2}\mathrm{tr}W^2\right) \\ &= N_W \exp\left(-\frac{1}{2\nu^2}\left(\sum_i W_{ii} + 2\sum_{i<j} W_{ij}\right)\right), \end{aligned} \tag{187}$$

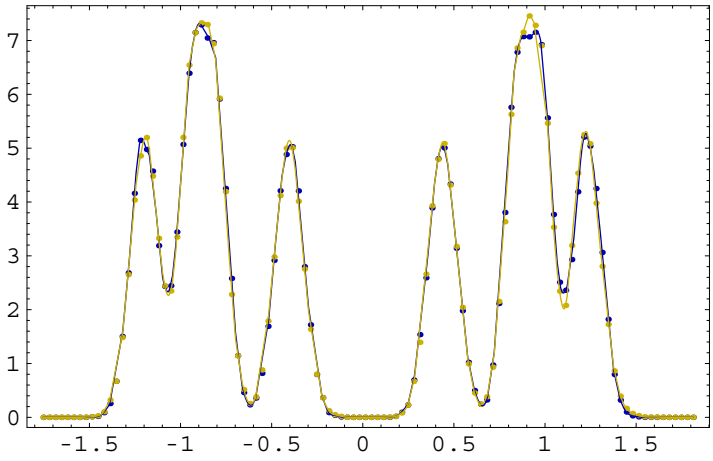

Figure 19: Same as Fig. 18 but for $2N = 8$. The smooth curves are cubic spline fits to histogram data.

where we have assumed W to be a real symmetric matrix.

There is, however, no reason to choose a gaussian over any other distribution from a physical point of view. As a matter of fact it can be argued that there exists one particular probability distribution (likely without such nice analytical properties) which corresponds to the details of the physical problem, apart from being restricted to the picture of an effective hamiltonian. If such a random matrix treatment is to be of any value, the answers to the questions we ask should be largely independent of the exact choice of our ensemble, $P(W)$.

This has been seen to be the case in a number of studies in random matrix theory. It is referred to as *universality*, and is quite akin to the central limit theorem which establishes the universality of the bell curve. The central limit theorem states that the distribution of the sum of random numbers drawn from an almost arbitrary random number distribution (a finite variance is a necessary condition) converges to a gaussian in the limit of large numbers. Similarly, universality in random matrix theory establishes that several spectral properties (the spectral density could be an example in certain cases) are independent of the distribution from which random matrices are drawn. [78, 79]

Figures 18 and 19 demonstrate the aforementioned universality. In one case, the matrix elements are drawn from a gaussian distribution as in (187) and in the other they are drawn from a flat distribution with the same variance. In the limit where the matrix size becomes large, it can be formally established that the spectral density and many other spectral properties such as eigenvalue correlators are independent of the distribution for individual matrix elements. It is striking to see that the same property holds remarkably for mesoscopic sized matrices, relevant for effective hamiltonians.

The spectral density can be computed analytically in the case where W are gaussian distributed hermitian matrices, but this is outside the scope of this manuscript. Some of the 'tools' necessary for such a computation may be found in [80, 81, 82].

Coherence Length in LH-II

Introduction

A simple model of electronic excitation and exciton -vibration coupling is employed to investigate the coherence length in the energy transfer within the B850 ring of LH-II. Path integral formulation of quantum statistical mechanics is used with Monte Carlo sampling of the closed imaginary time paths to calculate the mean coherence length. It's shown that localization occurs due to dynamic and static disorder and thermal averaging, with the dominant effect of the latter.

B850 ring of the LH-II of *Rs. molischianum* has 16 exciton states that are divided into two exciton bands. Degenerate 2nd and 3rd exciton states carry almost all of the oscillator strength which is a completely delocalized state over the whole ring at zero temperature. But under the biological conditions, it's still a subject of ongoing debate that whether it's still delocalized

Several experiments have estimated that coherence length varies between 1 and 4 chlorophyll monomers (BChl) [83, 84, 85, 86, 87]. Some groups claim that they found delocalized state at all temperatures [88, 89, 90]. Some says that incoherent energy transfer occurs at temperatures close to zero. There are some theoretical studies concerning the effect of static disorder on coherence, i.e. *Hu* et. al. found it to be small [91]. Mukamel's group investigated those effects on superradiance using adiabatic and polaron models [92]. A multilevel Redfield approach is used to follow the dynamics of the photo-excited state in the case of vibrational couplings and a dissipative bath by Sundström [92].

Imaginary time path integral formulation of quantum statistical mechanics [93] is employed to study these listed properties of excitations in LH-II. Monte Carlo path integral technique is highly efficient due to its ability to cover thermal averaging, static and dynamic disorder in a single calculation that leads to picture of coherence.

Model and Computational Procedure

Hamiltonian of LH-II B850 ring in the site basis, for fully symmetric case.

$$H_o \;=\; \varepsilon \sum_{i=1}^{n} |\alpha_i\rangle\langle\alpha_i| + \sum_{i\neq j}^{n} W_{ij}|\alpha_i\rangle\langle\alpha_j| \tag{188}$$

where $n = 16$, $|\alpha_i\rangle$ denotes excited state of the i'th BChl molecule and ε is its excitation energy. W_{ij} are the coupling terms between the BChl's. *Hu et. al.* used the following parameters, obtained by fitting eigenvalues to ZINDO electronic structure calculationresults.

$\varepsilon = 13059\,cm^{-1}$, $\quad W_{12} = v_1 = 809\,cm^{-1}$,

$W_{23} = v_2 = 377\,cm^{-1}$, $W_{13} = -152\,cm^{-1}$, $W_{24} = -109\,cm^{-1}$

Exciton-vibration coupling enters the Hamiltonian in a following way,

$$H \;=\; H_o \;+\; \sum_{j=1}^{n} \frac{p_j^2}{2m_j} \;+\; \frac{1}{2} m_j \omega_j^2 \left(x_j - \frac{c_j}{m_j \omega_j^2} \sum_{k=1}^{n} \sigma_k |\alpha_k\rangle\langle\alpha_k| \right)^2 \tag{189}$$

ω_j's and c_j's are harmonic modes and coupling constants of the dissipative bath that has collective characteristics contained in the spectral density,

$$J(\omega) \;=\; \frac{\pi}{2} \sum_j \frac{c_j^2}{m_j \omega_j} \delta\left(\omega - \omega_j\right) \tag{190}$$

which can be obtained from force autocorrelation function [94, 95, 96]. Since there is no available correlation function calculation for the LH-II yet,spectral density of a simple ohmic bath can be used instead.

$$J(\omega) \;=\; 2\pi\hbar\, \xi\, \omega e^{-\omega/\omega_c} \tag{191}$$

with a maximum at $\omega_c \;=\; 100\, cm^{-1}$ [103, 104]. ξ characterizes the reorganization energy between two neighbor BChl molecules given by

$$E_r \;=\; \frac{1}{\pi} \left(\sigma_k - \sigma_{k-1}\right)^2 \int_0^\infty \frac{J(\omega)}{\omega} d\omega \;=\; 2\pi\hbar\, \xi\, \omega_c \left(\sigma_k - \sigma_{k-1}\right)^2 \tag{192}$$

This value is different for interdimer and intradimer neighbor pairs of BChls. Because of the basence of detailed information, σ_k values are set to index number of BChl molecules with a periodic boundary condition $\sigma_{n+1} = \sigma_1$. Calculations are repeated for $\xi = 0, \xi = 0.1, \xi = 0.25$, no coupling, very weak coupling and weak coupling cases of corresponding reorganization energies 0, 20 and 50 cm^{-1}).

Coherences are associated with the off-diagonal elements of the density matrix in the site basis.and their contribution to canonical partition function provides a quantitative measure of how the off-diagonal elements are significant.Partition function is given by,

$$\mathrm{Z} \;=\; \mathrm{Tr}\, e^{-\beta H} \;=\; \sum_{i=1}^{n} \int_{-\infty}^{\infty} d\mathbf{x}\, \langle \alpha_i \mathbf{x} | e^{-\beta H} | \mathbf{x} \alpha_j \rangle \tag{193}$$

in the discretized path integral representation of N steps,

$$\begin{aligned} \mathrm{Z} \;=\; \sum_{k_1=1}^{n} \sum_{k_2=1}^{n} \ldots \sum_{k_N=1}^{n} \int_{-\infty}^{\infty} d\mathbf{x}_1 \int_{-\infty}^{\infty} d\mathbf{x}_2 \int_{-\infty}^{\infty} d\mathbf{x}_N \, \langle \alpha_N \mathbf{x}_N | e^{-\beta H/N} | \mathbf{x}_{N-1} \alpha_{N-1} \rangle \times \\ \ldots \times \langle \alpha_2 \mathbf{x}_2 | e^{-\beta H/N} | \mathbf{x}_1 \alpha_1 \rangle \langle \alpha_1 \mathbf{x}_1 | e^{-\beta H/N} | \mathbf{x}_N \alpha_N \rangle \end{aligned} \tag{194}$$

Imaginary time propagator can also be written as

$$\langle \alpha_i \mathbf{x}_i | e^{-\beta H/N} | \mathbf{x}_j \alpha_j \rangle \;=\; \langle \mathbf{x}_i | \, e^{-\beta/(2N)[H(\sigma_i) - H_o]} \, e^{-\beta/(2N)[H(\sigma_j) - H_o]} \, | \mathbf{x}_j \rangle \, \langle \alpha_i | e^{-\beta H_o/N} | \alpha_j \rangle \tag{195}$$

Last term is the exciton propagator which can be further simplified by using eigenstates Φ_k and eigenvalues E_k.

$$\langle\alpha_i|e^{-\beta H_o/N}|\alpha_j\rangle \;=\; \sum_{k=1}^{n}\langle\alpha_i|\Phi_k\rangle e^{-\beta E_k/N}\rangle\Phi_k|\alpha_j\rangle \tag{196}$$

$$\mathrm{Z} \;=\; \sum_{k_1=1}^{n}\sum_{k_2=1}^{n}\;...\;\sum_{k_N=1}^{n}\;\langle\alpha_N|e^{-\beta H_o/N}|\alpha_{N-1}\rangle...\langle\alpha_2|e^{-\beta H_o/N}|\alpha_1\rangle\,\langle\alpha_1|e^{-\beta H_o/N}|\alpha_N\rangle\;\times \\ \times F(\sigma_1,\sigma_2,...,\sigma_N) \tag{197}$$

where F is the influence functional and given by

$$F(\sigma_1,\sigma_2,...,\sigma_N) \;=\; \exp\left(-\sum_{k=1}^{N}\sum_{k'=1}^{N}\eta_{kk'}\sigma_k\sigma_{k'}\right) \tag{198}$$

$\eta_{kk'}$coefficients are obtained through integrals of spectral density hich has gaussian form and can be calculated analytically.

Final equation Z is sampled with the Metropolis procedure. Coherence length of each path in the sampling is given by

$$\ell \;=\; 2\sum_{k_1=1}^{n}\sum_{k_2=1}^{n}\;...\;\sum_{k_N=1}^{n}\;\langle\alpha_N|e^{-\beta H_o/N}|\alpha_{N-1}\rangle...\langle\alpha_2|e^{-\beta H_o/N}|\alpha_1\rangle\,\langle\alpha_1|e^{-\beta H_o/N}|\alpha_N\rangle\;\times \\ \times F(\sigma_1,\sigma_2,...,\sigma_N)\,[(\sigma_1-\sigma_c)^2+(\sigma_2-\sigma_c)^2+...+(\sigma_N-\sigma_c)^2] \tag{199}$$

where σ_c is the centroid of the closed path $\sigma_1,\sigma_2,...,\sigma_N$.

Static disorder can be implemented by replacing the parameter ε in the Hamiltonian by individual site energies, ε_i which chosen from a gaussian distribution. Then, mean coherence length is obtained through ensemble average of ℓ with respect to the fluctuation of the site energies ε_i's. Thus including the effect of static disorder adds only one more sampling step in the Monte Carlo simulation

Results

Coherence length in LH-II of *R. molischianum* shows the temperature dependence presented in Fig.1. Number of steps in one path is chosen as N=32. Number of Monte Carlo points per integration variable is 50000.

$$\sigma_k \;=\; \mathrm{int}\,(kn/N) \tag{200}$$

where $k=1,..,n$. Centroid of completely delocalized path $\sigma_c=(n+1)/2$ and the coherence length is

$$\ell \;=\; 2\sqrt{\frac{1}{n}\sum_{k=1}^{n}(k-\sigma_c)^2} \;=\; \sqrt{\frac{1}{3}(n^2-1)} \tag{201}$$

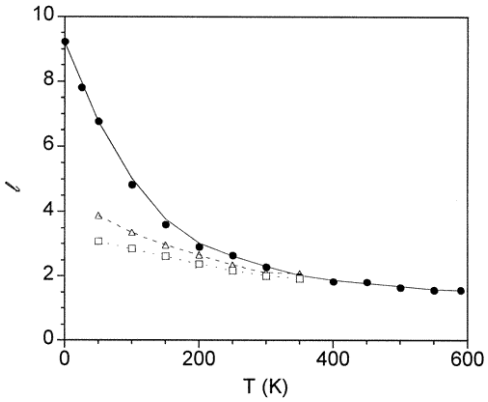

Figure 20: Coherence length vs. temperature for isolated ring ($\xi = 0$); (hollow triangles) very weak exciton-vibration coupling (ξ =0.1); (hollow squares) weak coupling ($\xi = 0.25$).

which gives $\ell = 9.22$ for $n = 16$. As seen in the Figure. 1, thermal averaging causes a dramatic localization of excitations. When we increase coupling to dissipative environment, localization gets stronger, i.e. for $\xi = 0.1$ coherence length is $\ell = 2.1$, for $\xi = 0.25$ coherence length is $\ell = 2.0$ at 300K.

Finally static disorder causes more localization , but considerably less than the thermal averaging.

Fig. 2 shows typical paths that are contributing the path integral expression of partition function most at low and room temperatures.

Conclusion

At low temperatures and in the absence of static disorder , excitations in LH-II are delocalized over the whole ring. But this picture drastically change when thermalization occurs. At room temperature , excitations only extend over 2-3 BChl molecules in the ring, which is 4 times smaller then that of 0 K.These results are in agreement with estimates of Fleming [97], van Grondelle [83, 102] and Sunström [100, 92, 98, 101]. Finally , if static disorder is taken into account, coherence length becomes shorter which must be the case in biological conditions.

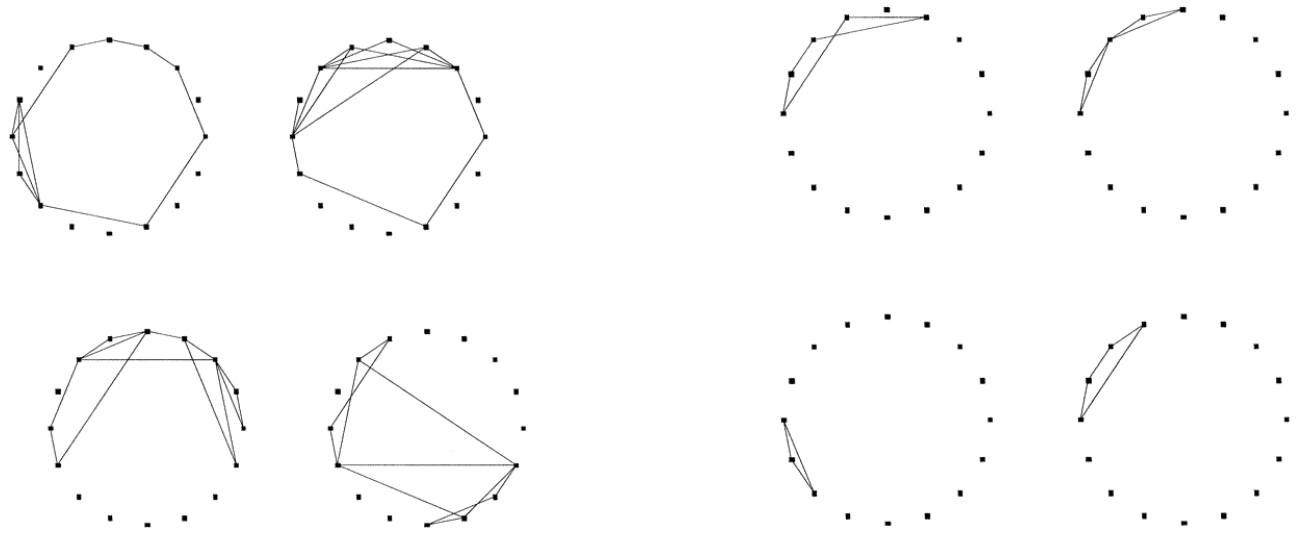

Figure 21: Typical paths for the isolated LH-II system ($\xi = 0$, no static disorder) at $T = 50\,K$ and $T = 300\,K$

Appendix: A quantum mechanical treatment of spectral transitions

Expression can be used also in case that one assumes a more rigerous description for the spectra $S_D(E)$ and $S_A(E)$. We want to provide here such description since its derivation is illuminating actually better the physics involved in the donor - acceptor excitation transfer process.

The goal in the following is to describe a two state quantum system coupled to a bath of quantum mechanical harmonic oscillators. We begin with the case that the bath contains only a single oscillator. Such situation is decribed by the Hamiltonian

$$\hat{H}_{\rm qo}^{(s)} = \begin{pmatrix} \hat{H}_r^{(s)} & v \\ v & \hat{H}_p^{(s)} + E \end{pmatrix} \tag{202}$$

where

$$\hat{H}_r^{(s)} = \frac{\hat{p}^2}{2m} + \frac{1}{2}m\omega^2 q^2 \tag{203}$$

$$\hat{H}_p^{(s)} = \frac{\hat{p}^2}{2m} + \frac{1}{2}m\omega^2 \left(q - \frac{c}{m\omega^2}\right)^2 \tag{204}$$

denote harmonic oscillator Hamiltonians of the *reactant* and *product* states. The additive energy term E denotes here a shift of the zero energy of the product state relative to the reactant state, e.g., denotes the redox energy difference between states AD and A^-D^+; *E will be considered a variable in the following*. If one wishes to describe a process going from the product (A^-D^+) state to the reactant (AD) state the sign of E in (202), representing the redox

energy difference, needs to be reversed. This property will be envoked below when we consider both processes, i.e., AD $\rightarrow$ A^-D^+ and $A^-D^+ \rightarrow$ AD.

The eigenstates and eigenvalues of the Hamiltonians (203, 204) are well-known from elementary quantum mechanics; they are

$$\langle q|n\rangle^{(\mathrm{r})} \;=\; \phi_n^{(\mathrm{r})}(q) \;=\; \left(\frac{\lambda}{\pi}\right)^{\frac{1}{4}} (2^n n!)^{-\frac{1}{2}} H_n(\sqrt{\lambda}q)\, e^{-\frac{1}{2}\lambda q^2} \tag{205}$$

$$\epsilon_n^{(\mathrm{r})} \;=\; \hbar\omega(n \,+\, \frac{1}{2}) \tag{206}$$

$$\langle q|n\rangle^{(\mathrm{p})} \;=\; \phi_n^{(\mathrm{p})}(q) \;=\; \left(\frac{\lambda}{\pi}\right)^{\frac{1}{4}} (2^n n!)^{-\frac{1}{2}} H_n(\sqrt{\lambda}(q - \frac{c}{m\omega^2}))\, e^{-\frac{1}{2}\lambda(q-c/m\omega^2)^2} \tag{207}$$

$$\epsilon_n^{(\mathrm{p})} \;=\; \hbar\omega(n \,+\, \frac{1}{2}) \tag{208}$$

where

$$\lambda \;=\; m\omega/\hbar \tag{209}$$

and where $H_n(y)$, $n = 0, 1, 2\ldots$ denote the Hermite polynomials. The reactant states describe an oscillator centered around $q \,=\, 0$, the product state an oscillator centered around

$$q_o \;=\; c/m\omega^2\,. \tag{210}$$

The propagator for the harmonic oscillator is well known. In case of the reactant state the propagator is

$$\begin{aligned}\langle q'|e^{-iH_r^{(s)}(t-t_o)/\hbar}|q\rangle \;\;=\;\; & \left[\frac{m\omega}{2i\pi\hbar\,\mathrm{sin}\omega(t-t_0)}\right]^{\frac{1}{2}} \;\times \\ & \exp\left\{\frac{im\omega}{2\hbar\,\mathrm{sin}\omega(t-t_0)}\,\left[\,(q'^2 \,+\, q^2)\,\mathrm{cos}\omega(t-t_0) \,-\, 2\,q'\,q\,\right]\right\}\,.\end{aligned} \tag{211}$$

This is equivalent to

$$\begin{aligned}\langle q'|e^{-iH_r^{(s)}(t-t_o)/\hbar}|q\rangle \;\;=\;\; & \left[\frac{\lambda}{2\pi\,\mathrm{sinh}\xi}\right]^{\frac{1}{2}} \;\times \\ & \exp\left\{-\frac{\lambda}{4}\left[\,(q' \,+\, q)^2\,\mathrm{tanh}\frac{\xi}{2} \,+\, (q' \,-\, q)^2\,\mathrm{coth}\frac{\xi}{2}\,\right]\right\}\,.\end{aligned} \tag{212}$$

$$\xi \;\;=\;\; i\,\omega(t \,-\, t_o)\,. \tag{213}$$

In case of the product state, the same expression applies after replacing $q \,\rightarrow\, q \,-\, q_o$ and $q' \,\rightarrow\, q' \,-\, q_o$.

The reactant states (205) are occupied in thermal equilibrium with probability

$$p_n^{(\mathrm{r})} \;=\; x^n(1 \,-\, x)\,, \quad x \,=\, e^{-\hbar\omega/kT}\,, \tag{214}$$

a result which is well-known from elementary statistical mechanics. The corresponding equilibrium state density matrix of the reactant state oscillator $\rho_o^{(\mathrm{r})}$ has the matrix elements

$$\left[\hat{\rho}_o^{(\mathrm{r})}\right]_{mn} \;=\; p_n^{(\mathrm{r})}\;\delta_{nm}\;. \tag{215}$$

The density matrix can also be written

$$\hat{\rho}_o^{(\mathrm{r})} \;=\; 2\sinh\left(\hbar\omega/2kT\right)\;e^{-H^{(\mathrm{r})}/kT}\;. \tag{216}$$

The transitions from reactant to product states are induced through the matrix elements v in (202). In case of electron transfer in proteins, the coupling is induced through electron tunneling between prosthetic groups in the protein. The corresponding energy values v are very small, usually of the order of 10^{-4} eV. As a result, reactant states $|n\rangle^{(\mathrm{r})}$ and product states $|m\rangle^{(\mathrm{p})}$ couple only when they are essentially degenerate. The overall rate of transfer from reactant states R to product states P is then

$$k_{qo}(R\to P) \;=\; \frac{2\pi}{\hbar^2}\,v^2\mathcal{S}_{qo}(E) \tag{217}$$

where

$$\mathcal{S}_{qo}(E) \;=\; \sum_{n,m=0}^{\infty} p_n^{(\mathrm{r})}\,|^{(\mathrm{r})}\langle n|m\rangle^{(\mathrm{p})}|^2\,\delta\left(\frac{E\;+\;\epsilon_m^{(\mathrm{p})}\;-\;\epsilon_n^{(\mathrm{r})}}{\hbar}\right) \tag{218}$$

is the so-called spectral line shape function.

We seek to express the line shape function (218) in a more compact form. For this purpose we use the identity

$$\delta\left(\frac{E\;+\;\epsilon_m^{(\mathrm{p})}\;-\;\epsilon_n^{(\mathrm{r})}}{\hbar}\right) \;=\; \frac{1}{2\pi}\int_{-\infty}^{+\infty} dt\;e^{itE/\hbar}\;e^{-it\epsilon_n^{(\mathrm{r})}/\hbar}\;e^{it\epsilon_m^{(\mathrm{p})}/\hbar}\;. \tag{219}$$

Employing the definition of the density matrix (215) one can write (218)

$$\mathcal{S}_{qo}(E) \;=\; \frac{1}{2\pi}\int_{-\infty}^{+\infty} dt\;e^{itE/\hbar}\;\sum_{n,m=0}^{\infty}\;{}^{(\mathrm{r})}\langle n|\,\hat{\rho}_o^{(\mathrm{r})}\,e^{-it\hat{H}_r^{(s)}/\hbar}\,|m\rangle^{(\mathrm{p})(\mathrm{p})}\langle m|\,e^{it\hat{H}_p^{(s)}/\hbar}\,|n\rangle^{(\mathrm{r})} \tag{220}$$

or, equivalently, using (216)

$$\mathcal{S}_{qo}(E) \;=\; \frac{1}{2\pi}\int_{-\infty}^{+\infty} dt\;e^{itE/\hbar}\;2\sinh\frac{\hbar\omega}{2kT}\;\mathrm{tr}\left(e^{-\hat{H}_r^{(s)}/kT}\,e^{-it\hat{H}_r^{(s)}/\hbar}\,e^{it\hat{H}_p^{(s)}/\hbar}\right)\;. \tag{221}$$

Expressing the trace as an integral over q' we conclude that the spectral line shape function is

$$\mathcal{S}_{qo}(E) \quad= \tag{222}$$
$$\frac{1}{2\pi}\int_{-\infty}^{+\infty} dt\;e^{itE/\hbar}\;2\sinh\frac{\hbar\omega}{2kT}\int_{-\infty}^{+\infty} dq\int_{-\infty}^{+\infty} dq'\;\langle q'|\,e^{-i(t\,-\,\hbar/kT)\hat{H}_r^{(s)}/\hbar}|q\rangle\langle q\,e^{it\hat{H}_p^{(s)}/\hbar}|q'\rangle\;.$$

The propagator (212) allows one to evaluate the line shape function (222). One employs

$$\langle q|\, e^{it\hat{H}_p^{(s)}/\hbar}|q'\rangle \;=\; \left[\frac{\lambda}{2\pi\sinh\eta_1}\right]^{\frac{1}{2}} \times \tag{223}$$

$$\times \exp\left\{-\frac{\lambda}{4}\left[(q'+q-2q_o)^2\tanh\frac{\eta_1}{2}+(q'-q)^2\coth\frac{\eta_1}{2}\right]\right\}.$$

$$\eta_1 \;=\; -i\omega t\,. \tag{224}$$

and, displacing time into the complex plane to account for the equilibrium (temperature T) density matrix,

$$\langle q'|\, e^{-i(t-\hbar/kT)\hat{H}_r^{(s)}/\hbar}|q\rangle \;=\; \left[\frac{\lambda}{2\pi\sinh\eta_2}\right]^{\frac{1}{2}} \times \tag{225}$$

$$\times \exp\left\{-\frac{\lambda}{4}\left[(q'+q)^2\tanh\frac{\eta_2}{2}+(q'-q)^2\coth\frac{\eta_2}{2}\right]\right\}.$$

$$\eta_2 \;=\; i\omega t-\hbar\omega/kT\,. \tag{226}$$

Inserting (223–226) into (222) results in the expression

$$\mathcal{S}_{qo}(E) \;=\; \frac{1}{2\pi}\int_{-\infty}^{+\infty} dt\; e^{itE/\hbar}\;\frac{\lambda\sinh\left(\frac{\hbar\omega}{2kT}\right)}{\pi\sqrt{\sinh\eta_1\,\sinh\eta_2}}\,I(t)\,. \tag{227}$$

where

$$I(t) \;=\; \int_{-\infty}^{+\infty}dq\int_{-\infty}^{+\infty}dq'\exp\left[-\alpha\,(t)(q+q')^2\;-\;\beta\,(q+q'-2q_o)^2\;-\;\gamma\,(q-q')^2\right] \tag{228}$$

$$\alpha \;=\; \frac{\lambda}{4}\tanh\frac{\eta_2}{2} \tag{229}$$

$$\beta \;=\; \frac{\lambda}{4}\tanh\frac{\eta_1}{2} \tag{230}$$

$$\gamma \;=\; \frac{\lambda}{4}\left(\tanh\frac{\eta_1}{2}\;+\;\tanh\frac{\eta_2}{2}\right) \tag{231}$$

Expression (227–231) for the spectral line shape function played an important role in the theory of spectral transitions of so-called F-centers in solids as reviewed in (Markham, 1959). The expression can be further simplified. For this purpose one transforms to new integration variables $u = q+q'$ and $u' = q-q'$. Noting that for the Jacobian holds $\partial(u,u')/\partial(q,q') = 2$, the integral (228) reads

$$I(t) \;=\; \frac{1}{2}\int_{-\infty}^{+\infty}du\int_{-\infty}^{+\infty}du'\,\exp\left[-\alpha\,(t)u^2\;-\;\beta\,(u-2q_o)^2\right]\,\exp\left[-\gamma\,u'^2\right]\,. \tag{232}$$

Completion of the square in the first exponent results in the expression

$$\begin{aligned} I(t) &= \frac{1}{2}\exp\left[-4q_o^2\left(\beta - \frac{\beta^2}{\alpha+\beta}\right)\right] \times \\ &\times \int_{-\infty}^{+\infty} du' \exp\left[-\gamma\, u'^2\right] \int_{-\infty}^{+\infty} du \exp\left[-(\alpha+\beta)\,(u-s)^2\right] . \end{aligned} \tag{233}$$

where

$$s = 2\beta q_o \,/\, (\alpha+\beta) . \tag{234}$$

Since $\mathrm{Re}(\gamma) > 0$ and $\mathrm{Re}(\alpha+\beta) > 0$ the Gaussian integrals can be evaluated in a straightforward way and one obtains

$$I(t) = \frac{\pi}{2\sqrt{\gamma(\alpha+\beta)}} \exp\left[-4q_o^2\left(\beta - \frac{\beta^2}{\alpha+\beta}\right)\right] . \tag{235}$$

We note here that this expression and, hence, $\mathcal{S}_{qo}(E)$ do not depend on the sign of q_o. This is to be expected due to the reflection symmetry of the harmonic oscillator potential. This behaviour implies, however, that a description of a process going from product states to reactant states does not require a change in the sign of q_o, even though that such change appears to be intuitively necessary.

Using definitions (229–231) and the properties of hyperbolic functions one can show

$$\frac{\lambda \sinh\left(\frac{\hbar\omega}{2kT}\right)}{2\sqrt{\sinh(\eta_1)\,\sinh(\eta_2)\,\gamma(\alpha+\beta)}} = 1 \tag{236}$$

One can also simplify the exponent in (235). One obtains

$$\beta - \frac{\beta^2}{\alpha+\beta} = \frac{\lambda}{4}\left(\tanh\frac{\eta_1}{2} - \frac{\tanh^2\frac{\eta_1}{2}}{\tanh\frac{\eta_1}{2} + \tanh\frac{\eta_2}{2}}\right) = \frac{\lambda}{4}\,\frac{\tanh\frac{\eta_1}{2}\tanh\frac{\eta_2}{2}}{\tanh\frac{\eta_1}{2} + \tanh\frac{\eta_2}{2}} . \tag{237}$$

Using $\tanh\alpha + \tanh\beta = \sinh(\alpha+\beta)/\cosh\alpha\cosh\beta$ the latter expression can be further rewritten

$$\begin{aligned} \beta - \frac{\beta^2}{\alpha+\beta} &= \frac{\lambda}{4}\,\frac{\sinh\frac{\eta_1}{2}\sinh\frac{\eta_2}{2}}{\sinh(\frac{\eta_1}{2}+\frac{\eta_2}{2})} = \frac{\lambda}{4}\,\frac{-\sinh\left(\frac{i\omega t}{2}\right)\,\sinh\left(\frac{i\omega t}{2}+\frac{\hbar\omega}{2kT}\right)}{\sinh\left(\frac{\hbar\omega}{2kT}\right)} \\ &= \frac{\lambda}{4}\,\frac{-\sinh\left(\frac{i\omega t}{2}\right)\,\left[\sinh\left(\frac{i\omega t}{2}\right)\,\cosh\left(\frac{\hbar\omega}{2kT}\right) + \sinh\left(\frac{\hbar\omega}{2kT}\right)\,\cosh\left(\frac{i\omega t}{2}\right)\right]}{\sinh\left(\frac{\hbar\omega}{2kT}\right)} \\ &= \frac{\lambda}{4}\left[\sin^2\frac{\omega t}{2}\coth\frac{\hbar\omega}{2kT} - i\cos\frac{\omega t}{2}\sin\frac{\omega t}{2}\right] \end{aligned} \tag{238}$$

which yields

$$\beta - \frac{\beta^2}{\alpha+\beta} = \frac{\lambda}{8}\left[(1-\cos\omega t)\coth\frac{\hbar\omega}{2kT} - i\sin\omega t\right] \tag{239}$$

Combining Eqs. (210, 227, 235, 236, 239) results in the final expression

$$\mathcal{S}_{qo}(E) \;=\; \frac{1}{2\pi}\int_{-\infty}^{+\infty} dt\, \exp\!\left[\, itE/\hbar \;-\; \frac{c^2}{2m\hbar\omega^3}\coth\!\frac{\hbar\omega}{2kT}\,(1-\cos\!\omega t) \;+\; i\,\frac{c^2}{2m\hbar\omega^3}\sin\!\omega t\,\right] \tag{240}$$

We note here that the rate for the reverse process, i.e., for going from the product state P to the reactant state R, is given by

$$k_{qo}(P\rightarrow R) \;=\; \frac{2\pi}{\hbar^2}\,v^2\mathcal{S}_{qo}(-E) \tag{241}$$

which differs from (217) solely through the sign of E.

The integral in (240) can be carried out and the line shape function expressed as a series of regular, modified Bessel functions $I_k(x)$. The result is

$$\mathcal{S}_{qo}(E) \;=\; \frac{e^{-\Lambda(1+2n_o)}}{\omega}\left(\frac{n_o+1}{n_o}\right)^{s_j/2}\;\sum_{k=-\infty}^{\infty}\;\delta\left(k-s(E)\right)\;I_k\left(2\Lambda\sqrt{n_o(n_o+1)}\right) \tag{242}$$

where $\Lambda \;=\; \frac{1}{2}m\omega^2 q_o^2/\hbar\omega \;=\; c^2/2m\hbar\omega^3$ is the so-called reorganization energy in units of vibrational quanta $\hbar\omega$, $n_o = e^{-\hbar\omega/kT}/(1-e^{-\hbar\omega_j/kT})$ is the average number of quanta thermally excited in the oscillator, and $s(E) = (E-\frac{1}{2}\hbar\omega)/\hbar\omega$ counts the number of oscillator levels up to energy E. The summation in (241) is over integers k such that one and only one term in the sum contributes anytime that $s(E)$ assumes an integer value.

References

[1] X. Hu and K. Schulten, Physics Today **50**, 28 (1997).

[2] X. Hu, A. Damjanović, T. Ritz, and K. Schulten, Proc. Natl. Acad. Sci. USA **95**, 5935 (1998), invited review.

[3] E. Hofmann *et al.*, Science **272**, 1788 (1996).

[4] M. Griffiths, W. Sistrom, G. Cohen-Bazire, and R. Y. Stanier, Nature **176**, 1211 (1955).

[5] W. R. Sistrom, M. Griffiths, and R. Y. Stanier, J. Cell. Comp. Physiol. **48**, 473 (1956).

[6] N. I. Krinsky, Pure Appl. Chem **51**, 649 (1979).

[7] R. J. Cogdell and H. A. Frank, Biochim. Biophys. Acta **895**, 63 (1987).

[8] N. A. Krinsky, in *The Survival of Vegetative Microbes*, edited by T. G. R. Gray and J. R. Postgate (Cambridge Univ. Press, Cambridge, 1976), pp. 209–239.

[9] G. McDermott *et al.*, Nature **374**, 517 (1995).

[10] J. Koepke *et al.*, Structure **4**, 581 (1996).

[11] A. P. Shreve *et al.*, Biochim. Biophys. Acta **1058**, 280 (1991).

[12] X. Hu, T. Ritz, A. Damjanović, and K. Schulten, J. Phys. Chem. B **101**, 3854 (1997).

[13] M. Kuki, H. Nagae, R. Cogdell, and Y. Koyama, Photochem. Photobiol. **59**, 116 (1994).

[14] P. Tavan and K. Schulten, J. Chem. Phys. **85**, 6602 (1986).

[15] B. S. Hudson, B. E. Kohler, and K. Schulten, in *Excited States*, edited by E. C. Lim (Academic Press, New York, 1982), Vol. 6, pp. 1–95.

[16] P. Tavan and K. Schulten, J. Chem. Phys. **70**, 5407 (1979).

[17] P. Tavan and K. Schulten, Phys. Rev. B **36**, 4337 (1987).

[18] P. Tavan and K. Schulten, in *Nonlinear Optical Properties of Polymers*, Vol. 109 of *Symposium Proceedings*, edited by A. J. Heeger, J. Orenstein, and D. Ulrich (Materials Research Society, Pittsburgh, 1988), pp. 163–170.

[19] T. Gillbro *et al.*, Photochem. Photobiol. **57**, 44 (1993).

[20] Y. Koyama, M. Kuki, P. Andersson, and T. Gillbro, Photochem. Photobiol. **63**, 243 (1996).

[21] B. W. Chadwick, C. Zhang, R. J. Cogdell, and H. A. Frank, Biochim. Biophys. Acta **893**, 444 (1987).

[22] A. P. Shreve, J. K. Trautman, T. G. Owens, and A. C. Albrecht, Chem. Phys. Lett. **178**, 89 (1991).

[23] M. Ricci, S. E. Bradforth, R. Jimenez, and G. R. Fleming, Chem. Phys. Lett. **259**, 381 (1996).

[24] T. Sashima, H. Nagae, M. Kuki, and Y. Koyama, (1998), unpublished.

[25] T. Förster, Ann. Phys. (Leipzig) **2**, 55 (1948).

[26] B. P. Krueger, G. D. Scholes, and G. R. Fleming, J. Phys. Chem. B **102**, 5378 (1998).

[27] H. Nagae, T. Kakitani, T. Katohi, and M. Mimuro, J. Chem. Phys. **98**, 8012 (1993).

[28] D.L.Dexter, J. Chem. Phys. **21**, 836 (1953).

[29] R. van Grondelle, J. Dekker, T. Gillbro, and V. Sundstrom, Biochim. Biophys. Acta **1187**, 1 (1994).

[30] K. R. Naqvi, Photochem. Photobiol. **31**, 523 (1980).

[31] C. S. Foote, Y. C. Chang, and R. W. Denny, J. Am. Chem. Soc. **92**, 5216 (1970).

[32] C. S. Foote, Free Radicals in Biology **2**, 85 (1976).

[33] M. Chessin, R. Livingston, and T. G. Truscott, Trans. Far. Soc. **62**, 1519 (1966).

[34] H. T. Witt, Quart. Rev. Biophys. **4**, 365 (1971).

[35] R. Bensasson, E. J. Land, and B. Maudinas, Photochem. Photobiol. **23**, 189 (1976).

[36] P. Mathis and J. Kleo, Photochem. Photobiol. **18**, 343 (1973).

[37] H. Claes and T. O. M. Nakayama, Zeit. Naturf. B **14**, 746 (1959).

[38] H. Claes, Biochem. Bicophys. Res. Comm. **3**, 585 (1960).

[39] M. M. Mathews-Roth and N. I. Krinsky, Photochem. Photobiol. **11**, 419 (1970).

[40] T. G. Monger, R. J. Cogdell, and W. W. Parson, Biochim. Biophys. Acta **449**, 136 (1976).

[41] K. Schulten, I. Ohmine, and M. Karplus, J. Chem. Phys. **64**, 4422 (1976).

[42] K. Schulten and M. Karplus, Chem. Phys. Lett. **14**, 305 (1972).

[43] W. Weber, Ph.D. thesis, Universität Zürich, Philosphische Fakultät II, Zürich, Switzerland, 1996.

[44] G. D. Scholes, K. P. Ghiggino, A. M. Oliver, and M. N. Padden-Row, J. Phys. Chem. **97**, 11871 (1993).

[45] S. Larsson, J. Am. Chem. Soc. **103**, 4034 (1981).

[46] *QUANTA 97*, Molecular Simulations Inc., Burlington, Massachusetts, 1997.

[47] J. Jortner, S. A. Rice, and J. L. Katz, J. Chem. Phys. **42**, 309 (1965).

[48] A. Szabo and N. Ostlund, *Modern quantum chemistry: Introduction to advanced electronic structure theory* (MacMillan, New York, 1982).

[49] *CERN Program Library Long Writeup Y250*, CERN, 1994.

[50] J. O. Hirschfelder and J. W. Linnett, J. Chem. Phys. **18**, 130 (1949).

[51] M. C. Zerner, M. G. Cory, X. Hu, and K. Schulten, J. Phys. Chem. (1998), in press.

[52] H. Wu and G. Small, J. Phys. Chem. B **102**, 888 (1998).

[53] L. Germeroth, F. Lottspeich, B. Robert, and H. Michel, Biochemistry **32**, 5615 (1993).

[54] H. Frank *et al.*, Pure Appl. Chem **68**, 2117 (1997).

[55] M. Mimuro *et al.*, Biochim. Biophys. Acta **1098**, 271 (1992).

[56] C. D. Caro, R. W. Visschers, R. van Grondelle, and S. Völker, J. Phys. Chem. **98**, 10584 (1994).

[57] A. Damjanović, T. Ritz, and K. Schulten, Phys. Rev. E. **59**, 3293 (1999).

[58] P. O. Anderson, T. Gillbro, L. Ferguson, and R. J. Cogdell, Photochem. Photobiol. **54**, 353 (1991).

[59] K. Sauer, J. R. L. Smith, and A. J. Schultz, J. Am. Chem. Soc. **88**, 2681 (1966).

[60] H. Frank and R. Cogdell, Photochem. Photobiol. **63**, 257 (1996).

[61] H. .A. Frank, R. L. Christensen, in *Anoxygenic Photosynthetic Bacteria*, edited by R. E. Blankenship, M. T. Madigan, and C. E. Bauer (Kluwer, Dordrecht, 1995), pp. 373–384.

[62] Z. Zhang *et al.*, Nature **392**, 677 (1998).

[63] R. Jimenez, S. Dikshit, S. Bradforth, and G. Fleming, J. Phys. Chem. **100**, 6825 (1996).

[64] D. Leupold *et al.*, Phys. Rev. Lett. **77**, 4675 (1996).

[65] P. D. Laible *et al.*, Biophys. J. **74**, 2623 (1998).

[66] W. Kuhlbrandt, in *Membrane Protein Structure: Experimental Approaches*, edited by S. White (Oxford University press, New York, 1994), pp. 206–223.

[67] J. B. Arellano, R. B. Raju, K. R. Naqvi, and T. Gillbro, Photochem. Photobiol. **68**, 84 (1998).

[68] J. Cizek, J. Paldus, and I. Hubac, Int. J. Quantum Chem. **8**, 951 (1974).

[69] J. Koutecky, J. Chem. Phys. **44**, 3702 (1996).

[70] R. Pariser, J. Chem. Phys. **24**, 250 (1956).

[71] W. F. Humphrey, A. Dalke, and K. Schulten, J. Mol. Graphics **14**, 33 (1996).

[72] Reddy, N.; Picorel, R., and Small, G. *J. Phys. Chem.*, 1992, 96, 6458.

[73] Somsen, O. J. G.; van Grondelle, R., and van Amerongen, H. *Biophys. J.*, 1996, 71, 1934.

[74] Nelson, M.; Humphrey, W.; Gursoy, A.; Dalke, A.; Kalé, L.; Skeel, R. D., and Schulten, K. *Int. J. Supercomput. Appl. High Perform. Comput.*, 1996. In press.

[75] Frisch, M. J.; Trucks, G. W.; H. B. Schlegel, G. E. S.; Robb, M. A.; Cheeseman, J. R.; V. G. Zakrzewski, J. A. M.; Stratmann, R. E.; Burant, J. C.; S. Dapprich, J. M. M.; Daniels, A. D.; Kudin, K. N.; Strain, M. C.; O. Farkas, J. T.; Barone, V.; Cossi, M.; Cammi, R.; Mennucci, B.; C. Pomelli, C. A.; Clifford, S.; Ochterski, J.; Petersson, G. A.; P. Y. Ayala, Q. C.; Morokuma, K.; Malick, D. K.; Rabuck, A. D.; K. Raghavachari, J. B. F.; Cioslowski, J.; Ortiz, J. V.; Stefanov, B. B.; Liu, G.; Liashenko, A.; Piskorz, P.; Komaromi, I.; Gomperts, R.; R. L. Martin, D. J. F.; Keith, T.; Al-Laham, M. A.; Peng, C. Y.; A. Nanayakkara, C. G.; Challacombe, M.; Gill, P. M. W.; Johnson, B. G.; W. Chen, M. W. W.; Andres, J. L.; Head-Gordon, M.; Replogle, E. S., and Pople, J. A. *Gaussian 98, Revision A7.* Gaussian Inc., Pittsburgh, PA, 1998.

[76] Mercer, I. P.; Gould, I. R., and Klug, D. R. *J. Phys. Chem. B*, 1999, 103, 7720.

[77] *Random Matrices, 2nd. ed.*, M. L. Mehta, 1991, Academic Press.

[78] G. Akemann, P. H. Damgaard, U. Magnea, and S. Nishigaki, *Nucl. Phys.* **B487** 721 (1997).

[79] M. K. Şener, and J. J. M. Verbaarschot, *Phys. Rev. Lett.*, **81** 248 (1998)

[80] J. J. M. Verbaarschot, H. A. Weidenmüller, and M. R. Zirnbauer, *Phys. Rep.* **129**, 367 (1985).

[81] T. Guhr, *J. Math. Phys.* **32**, 336 (1991).

[82] C. Itykson and J. B. Zuber, *J. Math. Phys.* **21**, 411 (1980).

[83] van Mourik, F.; Visschers, R. W.;v. Grondelle, R. *Chem. Phys. Lett.* **1992**, *193*, 1-7.

[84] Pullerits,T.;Visscher, K. J.; Hess, S.;Sundström, V.;Freibert, A.;Timpmann,K.; van Grondelle, R. *Biophys. J.* **1994**, *66*, 236

[85] Bradforth, S. E.;Jimenez, R.; van Mourik, F.; van Grondelle, R.;Fleming, G. R. *J. Phys. Chem.* **1995**, *99*, 16179.

[86] Monshouwer, R.; van Grondelle, R.; *Biochim. Biophys. Acta*, **1996**, *1275*, 70-75.

[87] Hess, S.;Chachisvilis, M.; Timpmann, K.; Jones, M.R.; Fowler, G. J. S.; Hunter, C. N.; Sundström,V. *Proc. Natl. Acad. Sci. U.S.A.* **1995**, *92*, 12333-12337.

[88] Xiao, W. H; Lin S.; Taguchi K. W.; Woodbury, N. W.*Biochemistry* **1994** ,*33* ,8313-8222.

[89] Wu H.-M.; Ratsep, M.; Lee, I-J.; Cogdell, R.J.; Small, G.J. *J. Phys. Chem. B* **1997**, *101*, 7654-7663.

[90] Kennis, J. T.; Streltsov, A.; Aartsma, T. J.; Nozawa, T.;Amesz J. *J. Phys. Chem.* **1996**, *100*, 2438-2442.

[91] Hu, X.; Ritz, T.; Damjanovic, A.; Schulten, K.; *J. Phys. Chem. B* **1997**, *101*, 3854-3871.

[92] Meier T.; Chao, Y.; Chernyak, V.; Mukamel, S. *J. Chem. Phys.* **1997**, *107*, 3876-3893.

[93] Feynman, R.P. *Statistical Mechanics*; Addison-Wesley; Redwood City, CA, 1972.

[94] Makri, N. *J. Phys. Chem* **1999**, *103*, 2823-2829

[95] Warshel, A.; Hwang, J.-K. *J. Chem. Phys.* **1986**, *84*, 4938-4957.

[96] Schulten, K.; Tesch, M. *J. Chem. Phys.* **1991**, *158*, 421-446

[97] Jimenez, R.; Dikshit, S.N.; Bradforth, S.E.; Fleming, G. R. *J. Phys. Chem.* **1996**, *100*, 6825-6834

[98] Kühn, O.; Sundström, V. *J. Chem. Phys.* **1997**, *107*, 4154-4164

[99] Kühn, O.; Sundström, V. *J. Phys. Chem. B* **1997**, *101*, 3432-3440

[100] Pullerits, T. ; Sundström, V. *Acc. chem. Res.* **1996**, *29*, 381-389

[101] Chachisvilis, M.; Kühn, O.; Pullerits, T.; Sundström, V. *J. Phys. Chem. B* **1997**, *101*, 7275-7283

[102] Monshouwer, R.; Abrahamsson, M.; van Mourik, F.; van Grondelle, R. *J. Phys. Chem. B* **1997**, *101*, 7241-7342

[103] Pullerits,T.; van Mourik, F.;Monshouwer, R.; Visschers, R. W.;van Grondelle, R. *J. Lumin.* **1994**, *58*, 168

[104] Visser, H. M.; Somsen, O. J. G.; van Mourik, F.; Lin, S.; van Stokkum, I. H. M.; van Grondelle, R. *Biophys. J.* **1995**, *69*, 1083